Male mammalian meiosis and spermiogenesis is critically dependent on the shared functions of the katanins KATNA1 and KATNAL1

Authors

Jessica EM Dunleavy[1], Maddison Graffeo[1], Kathryn Wozniak[2], Anne E O'Connor[1], D. Jo Merriner[1], Joseph Nguyen[1], Ralf B Schittenhelm[3], Brendan J Houston[1], Moira K O'Bryan[1]

[1]School of BioSciences and Bio21 Institute, Faculty of Science, The University of Melbourne, VIC, 3010, Australia. [2]Monash Biomedicine Discovery Institute and The Department of Anatomy and Developmental Biology, Monash University, Melbourne VIC, 3800, Australia [3]Monash Proteomics & Metabolomics Facility, Department of Biochemistry and Molecular Biology, Biomedicine Discovery Institute, Monash University, Clayton VIC, 3800, Australia

***Correspondence:** Jessica.dunleavy@unimelb.edu.au

Summary

Katanin microtubule severing enzymes are potent M-phase regulators in oocytes and somatic cells. How the complex, and evolutionarily critical, male mammalian meiotic spindle is sculpted remains unknown. Here, using multiple single and double gene knockout mice, we reveal that the canonical katanin A-subunit, KATNA1, and its close paralogue, KATNAL1, together execute multiple aspects of meiosis. We show KATNA1 and KATNAL1 collectively regulate the male meiotic spindle, cytokinesis and midbody abscission, in addition to diverse spermatid remodelling events, including Golgi organisation, and acrosome and manchette formation. We also define KATNAL1-specific roles in sperm flagella development, manchette regulation, and sperm-epithelial disengagement. Finally, using proteomic approaches we define the KATNA1, KATNAL1, and KATNB1 mammalian testis interactome, which includes a network of cytoskeletal and vesicle trafficking proteins. Collectively, we reveal the presence of multiple katanin A-subunit paralogs in mammalian spermatogenesis allows for 'customized cutting' via neofunctionalization and protective buffering via gene redundancy.

Keywords: Meiotic spindle, spermatogenesis, microtubule severing, manchette, axoneme, acrosome, HTCA, male fertility, vesicle transport, spermiation

Introduction

The katanins are an evolutionary conserved family of microtubule (MT) severing proteins that were first identified as an essential meiosis regulator in *Caenorhabditis elegans* oocytes[1]. Since then, they have been established as a nuanced regulator of MTs, able to employ the same action (physical removal of tubulin heterodimers from the MT lattice) to amplify, disassemble or even strengthen MTs (for reviews see McNally et al.[2] and Sarbanes et al.[3]). At a cellular level these actions drive rapid MT remodelling events required in many processes including ciliogenesis,

40 cell division and differentiation, and allow fine tuning of homeostatic MT structures and
41 processes.
42
43 The canonical katanin complex consists of an AAA ATPase catalytic severing enzyme
44 KATNA1 (aka p60 or A-subunit) and a WD40-repeat containing regulatory subunit KATNB1
45 (aka p80 or B-subunit) and is conserved across most eukaryotes. In its active ATP bound state,
46 the A-subunit forms a spiral hexamer which binds MTs and threads the C-terminal tail (CTT)
47 of a tubulin subunit through its central pore. An ATP-driven conformational change in the
48 hexamer, causes an extractive force on the tubulin CTT removing the tubulin heterodimer from
49 the lattice. In higher eukaryotes, the B-subunit is not essential for A-subunit severing activity,
50 however it increases MT affinity and severing efficiency, and at a cellular level is often
51 essential for A-subunit localisation[2]. In vertebrates, *Drosophila,* and unicellular ciliates,
52 paralogous A-subunits, KATNAL1 and KATNAL2 are present, and an additional WD40-less
53 KATNB1 paralog, KATNBL1 is present in vertebrates. KATNAL1 is highly similar in
54 sequence and domain architecture to KATNA1[2] and has been shown to possess MT-severing
55 activity[4]. KATNAL2 however, outside of the conserved AAA ATPase MT severing domain,
56 differs in domain architecture to KATNA1 and KATNAL1[2] and in standard MT severing
57 assays did not exhibit MT severing activity[4,5]. This aside, loss of KATNAL2 function in mouse
58 spermatogenesis resulted in phenotypes consistent with loss of MT severing[5].
59
60 Across eukaryotes, the regulation of cell division is a defining feature of katanin action. In *C.*
61 *elegans* oocytes, the orthologues of KATNA1 and KATNB1, MEI-1 and MEI-2 drive
62 formation of the bipolar spindle in meiosis I via MT amplification, and subsequently regulate
63 spindle length, function and positioning[2,6] and in meiosis II, mediate spindle disassembly[7].
64 KATNA1 has also been shown to regulate female meiotic spindle length in *Xenopus laevis* and

65 *Xenopus tropocalis*[8], and in cultured mouse oocytes KATNAL1 depletion results in abnormally
66 long meiotic spindles and an increase in multipolar spindles [9]. Likewise, in mitosis, katanin
67 A-subunits have variously been shown to regulate mitotic spindle size/shape, polarity, density
68 and orientation, and drive midbody abscission during cytokinesis in species ranging from
69 unicellular ciliates and plants to mammalian cell lines[2,6,10]. Despite these data, the contribution
70 of katanin proteins to male meiosis has received little attention. The requirement, and identity,
71 of katanin A-subunits in male mammalian meiosis has not been directly tested, although data
72 from loss-of-functions in the regulatory, B-subunit, KATNB1, strongly suggest katanin-
73 mediated MT severing is required[11,12].
74
75 Herein we aimed to identify the function of katanin-A subunits in male mammalian meiosis.
76 Using a suite of single and double katanin A-subunit deletion mice, we reveal KATNA1 and
77 KATNAL1 collectively regulate male meiosis, wherein they refine metaphase spindle structure
78 and chromosome alignment and drive accurate chromosome segregation. We show their
79 functions extend into haploid germ cell development (spermiogenesis), a process that
80 necessitates the development of several specialised MT structures. We identify KATNA1 and
81 KATNAL1 as global regulators of spermatid MTs required to restrain MT bulk, and as well as
82 identifying several structure/process specific roles, including in Golgi function and acrosome
83 biogenesis. We further identify KATNAL1 specific roles in cytokinesis during meiosis, in the
84 formation of the sperm head-to-tail coupling apparatus (HTCA) and axoneme, in sperm head
85 sharping via manchette MT dynamics and dissolution, and in sperm release (spermiation).
86 During spermatogenesis, we reveal KATNAL1 can fully functionally compensate for loss of
87 KATNA1. In contrast, we show KATNA1 can only partially compensate for KATNAL1 loss,
88 and there is no functional compensation between KATNA1 and KATNAL2 in the mouse testis.
89 Finally, using an *in vivo* immunoprecipitation (IP)-mass spectrometry (MS) approach, we

90 reveal these diverse cellular functions are mediated by an equally diverse set of KATNA1,
91 KATNAL1 and KATNB1 testis interacting partners, including MT associated proteins,
92 regulators of actin dynamics and organisation, vesicle-transport proteins including multiple
93 Rab GTPase family members, and essential mediators of male meiosis and acrosome
94 biogenesis. Collectively these results reveal the complex reliance of spermatogenesis on
95 katanin function and the precise neofunctionalization of A-subunits required to achieve normal
96 sperm function and morphology.
97

98 **Results**

99 **KATNA1 is not essential for male fertility in the mouse**

100 Despite the clear necessity for the dynamic regulation of MT structures during meiosis, and
101 data showing that the loss of the KATNB1 leads to notable defects in meiosis[11,12], the 'effector'
102 A-subunit is unknown. Data from *C. elegans* reveal the KATNA1 orthologue MEI-1 is a key
103 regulator of female meiosis. To test the hypothesis that KATNA1 serves an analogous function
104 in male meiosis, we generated a *Katna1* germ cell specific knockout mouse model
105 (*Katna1*$^{GCKO/GCKO}$, Fig S1A-C). As shown in Fig S1D, *Katna1* mRNA expression was reduced
106 by 91.77% in *Katna1*$^{GCKO/GCKO}$ spermatocytes compared to *Katnal1*$^{Flox/Flox}$ controls. Loss of
107 KATNA1 at the protein level was confirmed via immunolabelling of testis sections (Fig S1E).
108

109 *Katna1*$^{GCKO/GCKO}$ mice had normal body weight (Fig S2A) and unexpectedly were fertile.
110 *Katna1*$^{GCKO/GCKO}$ mice exhibited normal testis weight, testis daily sperm production and
111 epididymal sperm content (Fig S2B,C,D). Histological assessment of the male reproductive
112 tract in *Katna1*$^{GCKO/GCKO}$ mice revealed normal progression of germ cells through all phases of
113 spermatogenesis and the presence of sperm in the epididymis (Fig S2E,F,G). Sperm from
114 *Katna1*$^{GCKO/GCKO}$ mice were cytologically comparable to those from *Katnal1*$^{Flox/Flox}$ controls

115 (Fig S2H) and were functionally competent, as exhibited by normal fertility when mated with
116 wild-type females (8.2 pups per copulatory plug in *Katna1*$^{GCKO/GCKO}$ versus 7.1 pups in
117 controls, P=0.0969). Collectively, these data reveal KATNA1 is dispensable for mammalian
118 spermatogenesis.
119
120 **Germ cell derived KATNAL1 is required for optimal male fertility in mice**
121 We next sought to explore the requirement in meiosis for the non-canonical katanin A-subunit,
122 KATNAL1. A role for KATNAL1 in the somatic Sertoli cell population of the testis has been
123 defined [13], but a specific role in male meiosis has not been tested. To do this we generated a
124 *Katnal1* germ cell specific knockout mouse model (*Katnal1*$^{GCKO/GCKO}$, Fig S3A,B). Successful
125 ablation of *Katnal1* gene expression was confirmed by qPCR, western blotting of purified germ
126 cells and immunolabeling of testis sections (Fig 3C-E). There was a 99.56% reduction in
127 *Katnal1* mRNA in *Katnal1*$^{GCKO/GCKO}$ compared to *Katnal1*$^{Flox/Flox}$ germ cells.
128

129 *Katnal1*$^{GCKO/GCKO}$ males exhibited normal mating frequency but were subfertile siring 84%
130 fewer pups per copulatory plug than *Katnal1*$^{Flox/Flox}$ controls (6.9 ± 3.1SD pups / plug sired by
131 *Katnal1*$^{Flox/Flox}$ males versus 1.4 ± 1.6SD pups / plug sired by *Katnal1*$^{GCKO/GCKO}$ males,
132 P=0.0151). As outlined below, this subfertility was due to a dramatic reduction in sperm
133 number, and abnormal sperm morphology and motility. *Katnal1*$^{GCKO/GCKO}$ mice had body and
134 testis weights comparable to *Katnal1*$^{Flox/Flox}$ mice (Fig 1A,B). Likewise, the number of
135 apoptotic germ cells per seminiferous tubules was not significantly different between
136 *Katnal1*$^{Flox/Flox}$ and *Katnal1*$^{GCKO/GCKO}$ mice (Fig 1D). Despite this, *Katnal1*$^{GCKO/GCKO}$ testis
137 daily sperm production was reduced by 42.3% compared to *Katnal1*$^{Flox/Flox}$ mice (Fig 1C),
138 indicative of germ cell loss in the later steps of spermiogenesis, when spermatids contribute
139 minimally to the overall weight of the testis. Finally, epididymal sperm content was reduced

140 by 73.7% compared to *Katnal1*$^{Flox/Flox}$ mice (Fig 1D). This reveals that germ cell derived
141 KATNAL1 is required for optimal spermiogenesis and, as evidenced by the more severe
142 reduction in epididymal sperm content relative to DSPs, for their ultimate release from the
143 seminiferous epithelium via the process of spermiation. Assessment of *Katnal1*$^{GCKO/GCKO}$
144 seminiferous tubule histology confirmed the abnormal retention of elongated spermatids in
145 stage IX tubules (Fig 1G).

146

147 While all germ cell types were present in the *Katnal1*$^{GCKO/GCKO}$ seminiferous epithelium, many
148 *Katnal1*$^{GCKO/GCKO}$ tubules contained fewer germ cells, notably spermatids, compared to
149 *Katnal1*$^{Flox/Flox}$ mice (Fig 1E,F). Areas of Sertoli cell-only tubules were observed and gaps
150 between adjacent Sertoli cells were frequently seen in *Katnal1*$^{GCKO/GCKO}$ but never in
151 *Katnal1*$^{Flox/Flox}$ (Fig 1E,F). Epididymal histology was consistent with the presence of fewer
152 sperm in *Katnal1*$^{GCKO/GCKO}$, in addition to the presence of prematurely sloughed germ cells in
153 *Katnal1*$^{GCKO/GCKO}$, but not *Katnal1*$^{Flox/Flox}$, mice (Fig 1H). Of note, immunolabelling testis
154 sections for the Sertoli cells specific β-tubulin isoform, TUBB3, confirmed the origins of the
155 reduced spermatogenic output in the *Katnal1*$^{GCKO/GCKO}$ were distinct from those of the
156 previously characterised *Katnal1*$^{1H/1H}$ hypomorphic mouse model where extensive disruption
157 of the Sertoli cell MT cytoskeleton was seen[13]. In contrast, in *Katnal1*$^{GCKO/GCKO}$ testis sections
158 TUBB3 localisation was comparable to *Katnal1*$^{Flox/Flox}$ (Fig S4A-B). These data reveal that
159 KATNAL1 plays an essential role in the regulation of MTs in both Sertoli and germ cells.

160

161 Of the sperm present in the epididymides of *Katnal1*$^{GCKO/GCKO}$ mice, almost all were
162 morphologically abnormal (97.1% in *Katnal1*$^{GCKO/GCKO}$ versus 23.9% in *Katnal1*$^{Flox/Flox}$, Fig
163 1I,J). Abnormalities included in head shape (97.1% in *Katnal1*$^{GCKO/GCKO}$ versus 11.3% in

164 *Katnal1*$^{Flox/Flox}$), head position (36.4% versus 2.3%), coupling between the head and tail
165 (decapitation, 34.7% versus 11.5%), mid-pieces structure (coiling, 14.4% versus 0.0%) and
166 mitochondrial sheath structure (3.9% versus 0.0%) (Fig 1J). Moreover, of those sperm found
167 in *Katnal1*$^{GCKO/GCKO}$ epididymides, there was a 20.2% reduction in the ability for motility and
168 a 52.9% reduction in progressive motility in the absence versus presence of KATNAL1 (Fig
169 2K,L). Considering the reduction in sperm number in *Katnal1*$^{GCKO/GCKO}$ mice, this equates to
170 an 87.6% reduction in the total number of progressively motile sperm in *Katnal1*$^{GCKO/GCKO}$
171 compared to *Katnal1*$^{Flox/Flox}$ mice. Collectively these phenotypes reveal germ cell derived
172 KATNAL1 is required for normal spermatogenesis and optimal male fertility.
173
174 **KATNAL1 regulates chromosome alignment, segregation and cytokinesis during male**
175 **meiosis**
176 The reduction in post-meiotic germ cells in *Katnal1*$^{GCKO/GCKO}$ seminiferous tubules indicated a
177 variably penetrant meiotic defect. To assess *Katnal1*$^{GCKO/GCKO}$ meiotic spindles, testis sections
178 were stained for α-tubulin as a component of MTs (Fig 2A,B). As seen in *Katnal1*$^{Flox/Flox}$ stage
179 XII tubules, metaphase I and II meiotic spindle MTs typically project from the two opposing
180 spindle poles in a narrow and uniform angle to tightly align chromosomes/chromatids along
181 the metaphase plate (Fig 2Aa,2Ba-c). In *Katnal1*$^{GCKO/GCKO}$ stage XII tubules, the vast majority
182 of metaphase spindles displayed normal spindle architecture and normal MT spindle density
183 (Fig 2Ae, Bf-h). Chromosomal alignment at the metaphase plate, however, was noticeably
184 abnormal in many *Katnal1*$^{GCKO/GCKO}$ metaphase spermatocytes, with misaligned chromosomes
185 often observed (Fig 2A,Bf-g, green arrowheads). These defects did not however prevent
186 progression to anaphase, with no increase in metaphase arrest and apoptosis in stage XII-I
187 seminiferous tubules in *Katnal1*$^{GCKO/GCKO}$ compared to *Katnal1*$^{Flox/Flox}$ mice (Fig 2A,E-J).
188

189 Similarly, KATNAL1 loss in germ cells did not prevent spermatocyte progression through
190 anaphase and telophase. Specifically there was no discernible increase in *Katnal1*$^{GCKO/GCKO}$
191 spermatocytes stalling in anaphase or telophase or undergoing apoptosis (Fig 2A,E-J). Instead,
192 anaphase and telophase defects in *Katnal1*$^{GCKO/GCKO}$ meiosis led to the production of abnormal
193 haploid germ cells. In anaphase I and II, spindle MTs undergo poleward shortening, allowing
194 them to pull chromosomes toward opposing poles in a coordinated manner, as observed in
195 *Katnal1*$^{Flox/Flox}$ anaphase spermatocytes (Fig 2Ab,Bd-e). In *Katnal1*$^{GCKO/GCKO}$ anaphase
196 spermatocytes however, uneven segregation of chromosomes was often observed, with lagging
197 chromosomes commonly seen (Fig 2Af, Bi-j, green arrowheads). Consistent with uneven
198 chromosome segregation in anaphase, many round spermatids possessed abnormally large
199 nuclei (Fig 2Cb-c, yellow arrowheads). During telophase and cytokinesis midbodies were
200 present in *Katnal1*$^{GCKO/GCKO}$ and were comparable to those in *Katnal1*$^{Flox/Flox}$ spermatocytes
201 (Fig 2Ac,g). However, a subset of the resulting spermatids was binucleated (Fig 2Cd,e, orange
202 arrowheads), and as detailed below sperm/spermatids with multiple axonemes (Fig 3C) and
203 supernumerary centrioles (Fig 3Db, red arrowhead) were often observed. This indicates that
204 while midbodies do form in the absence of *Katnal1*, KATNAL1 plays a key role its remodelling
205 into an intracytoplasmic bridge and the maintenance of individual daughter spermatids.
206 Binucleated spermatids were never observed in *Katnal1*$^{Flox/Flox}$ tubules.
207
208 These data reveal KATNAL1 regulates MT-chromosome attachment and/or metaphase spindle
209 dynamics but is dispensable for MT generation and pruning during spindle biogenesis in male
210 meiosis. Moreover, our data show KATNAL1 greatly facilitates accurate chromosome
211 segregation during anaphase and midbody function and disassembly during cytokinesis in
212 either meiosis I and/or meiosis II.
213

214 **KATNAL1 regulates flagella and manchette formation in male germ cells**

215 As detailed above, of the epididymal sperm that were produced in *Katnal1*$^{GCKO/GCKO}$ mice
216 97.1% were morphologically abnormal revealing that KATNAL1 is required during spermatid
217 differentiation (spermiogenesis) (Fig 1I,J). One of the first processes to commence in
218 spermiogenesis is acrosome formation, and our recent data identified MT severing as a
219 potential regulator of this process [11]. The identity of the involved MT severing A-subunit
220 remains unknown. Acrosome formation was overtly normal in *Katnal1*$^{GCKO/GCKO}$ mice
221 compared to *Katnal1*$^{Flox/Flox}$ controls, indicating KATNAL1 is not essential for this process
222 (Fig S4C).

223

224 Multiple abnormalities were however observed in *Katnal1*$^{GCKO/GCKO}$ mouse sperm tails and the
225 head-to-tail coupling apparatus (HTCA), including abnormal reticulation of the sperm head,
226 decapitation, coiling of the sperm tail mid-piece and mitochondrial sheath defects, in addition
227 to reduced sperm motility. Staining of *Katnal1*$^{GCKO/GCKO}$ testis sections for acetylated tubulin,
228 as a marker of stable MTs, revealed axonemal MTs were present in sperm tails (Fig 3B),
229 however analysis via transmission electron microscopy (TEM) revealed a range of axoneme
230 and accessory structure abnormalities (Fig 3C). In *Katnal1*$^{GCKO/GCKO}$ mice, sperm flagella
231 axonemes often lacked the typical 9+2 MT doublet arrangement observed in controls (Fig
232 3Ca,d,g). Instead MT doublets were often missing (Fig 3Ce,f,h, yellow asterisks), ectopically
233 located (Fig 3C, red arrowheads) or in many cases supernumerary MT doublets were present
234 (Fig 3Cc,l, white arrowheads). In the most dramatic instances, and consistent with the failures
235 in cytokinesis, multiple axonemes, often each with associated accessory structures, were
236 observed within one cell (Fig 3Cb,j-l). The abnormalities in MT doublet number and location
237 were typically accompanied by defects in outer dense fiber (ODF) number and location (Fig
238 3C). In wild-type sperm, the mid-piece contains 9 ODFs closely associated with the 9 outer

239 MT doublets of the axoneme (Fig 3Ca). In the principal piece ODFs 3 and 8 are replaced by
240 the longitudinal columns of the fibrous sheath (Fig 3Cd). In *Katnal1*$^{GCKO/GCKO}$ mice however,
241 sperm tail ODFs 3 and/or 9 frequently persisted into the principal piece (Fig 3Cb,c, green
242 arrowheads). In *Katnal1*$^{GCKO/GCKO}$ mouse sperm tails wherein some or all axoneme MTs were
243 missing, ODFs were often also missing (Fig 3Ce,f). Consistent with the coiled mid-pieces and
244 mitochondrial sheath defects observed in some sperm from *Katnal1*$^{GCKO/GCKO}$ mice, TEM
245 revealed that in many sperm the mitochondria were not properly organised into a helical sheath
246 (Fig 3Cj). Fibrous sheath development in *Katnal1*$^{GCKO/GCKO}$ sperm however, appeared normal
247 in most cells (Fig 3C). Finally, in some sperm, only disorganised fragments of sperm tail
248 components were observed indicative of degenerating cells (Fig 3Cm). Collectively, these data
249 reveal KATNAL1-mediated MT severing regulates the assembly and potentially stability of
250 axoneme MT doublets, and that KATNAL1 contributes to the development of the
251 mitochondrial sheath and ODFs, but not the fibrous sheath. These data are consistent with
252 defects in cargo/organelle delivery to and along the growing sperm tail. Indeed, there is an
253 increasing of body of evidence (reviewed by Pleuger et al.[14]) that mitochondria and ODFs rely
254 on MT-based transport mechanisms for their delivery into the sperm tail.
255
256 The frequent decapitation or hyper-extension of sperm heads, in sperm from *Katnal1*$^{GCKO/GCKO}$
257 males, indicates the HTCA was weak and/or improperly formed in the absence of KATNAL1.
258 Moreover, TEM of round and elongated spermatids revealed a range of HTCA abnormalities
259 in *Katnal1*$^{GCKO/GCKO}$ mice compared to controls (Fig 3D). In *Katnal1*$^{Flox/Flox}$ mice, spermatid
260 HTCAs were easy to find in testis sections via TEM. As expected, they contained a proximal
261 centriole coupled to the nucleus via the basal plate and capitulum, a distal centriole coupled to
262 the plasma membrane and continuous with the axoneme, and the surrounding segmented
263 columns which are continuous with the ODFs (Fig 3Da,f). In *Katnal1*$^{GCKO/GCKO}$ mice, however

264 normal HTCAs were rare (Fig 3Db,g). In most spermatids, HTCAs were abnormal (Fig 3Dc-
265 e, h-j). In some cells, the HTCA and associated axoneme was present, but not attached to the
266 nucleus (Fig 3Dc,h, yellow arrowheads), while in others the basal plate could be seen
267 associated with the nucleus, but the rest of the HTCA was absent (Fig 3Dg). Consistent with
268 this data, immunolabelling of sperm for SUN5, which is an essential component of the LINC
269 complex that physically docks the sperm centrosome to the nucleus, revealed a 57.2%
270 reduction in sperm from *Katnal1*$^{GCKO/GCKO}$ males containing SUN5 at the HTCA compared to
271 sperm from *Katnal1*$^{Flox/Flox}$ mice (Fig S4D,E). These data suggest that KATNAL1 regulated-
272 MTs are either required to fortify the connection between the basal plate and the nucleus or are
273 required for the delivery and deposition of essential components of the HTCA. Our data also
274 suggest that SUN5 is delivered to the HTCA via KATNAL1-regulated MTs.
275
276 Abnormal head shape was the most frequent morphological abnormality present in the sperm
277 of *Katnal1*$^{GCKO/GCKO}$ mice. Instead of the normal hook shape exhibited in 88.75% of
278 *Katnal1*$^{Flox/Flox}$ mouse sperm, 34% of *Katnal1*$^{GCKO/GCKO}$ mouse sperm heads exhibited a
279 'hammerhead' shape and 62% exhibited a 'knobby' head phenotype (Fig 1I, S4F,G). Abnormal
280 head shaping became apparent during nuclear elongation (Fig 3E) and were consistent with
281 defects in manchette function, where the manchette is a transient MT-based structure which
282 sculpts the distal half of the spermatid head. As shown in Fig 3F in wild-type mice the
283 manchette forms in step 8-9 spermatids (stage VIII-IX seminiferous tubules), before migrating
284 distally while simultaneously constricting to shape the spermatids head during steps 10-12
285 (stages X-XII; Fig 3F). In steps 13-14 (stage I-III) the manchette is dissembled (Fig 4F). In
286 spermatids from *Katnal1*$^{GCKO/GCKO}$ mice, manchettes formed at step 8-9 but were abnormally
287 elongated. Elongation became increasingly pronounced as spermatid development continued
288 and was associated with a failure of manchette perinuclear ring migration down the sperm head,

289 but continued constriction, and resulting in a 'knobby head' phenotype (Fig 4G). Finally,
290 manchette disassembly in steps 13-14 was delayed in the absence of KATNAL1 (Fig 4F).
291 Collectively, these results reveal KATNAL1-mediated MT severing is required to regulate
292 manchette MT length, migration and disassembly.
293
294 **KATNA1 and KATNAL1 compensate for each other in male meiosis and spermiogenesis**
295 Given the apparently normal fertility in *Katna1*$^{GCKO/GCKO}$ and residual fertility in
296 *Katnal1*$^{GCKO/GCKO}$ mice, we sought to explore the possibility of functional compensation,
297 between KATNA1 and its paralogs KATNAL1 and KATNAL2 in the testis. This is a
298 particularly critical question for meiosis wherein the identity of the critical A-subunit(s)
299 remains unknown. As reported previously, *Katnal2* loss has no apparent effect on male meiosis
300 but does result in male infertility due to severe sperm developmental defects[5]. To test for
301 redundancy, we generated (1) *Katna1* and *Katnal1* double germ cell knockout mice
302 (*Katna1/al1*$^{GCKO/GCKO}$) and (2) double *Katna1* germ cell and *Katnal2* knockout mice
303 (*Katna1*$^{GCKO/GCKO}$*/al2*$^{KO/KO}$). The *Katna1*$^{GCKO/GCKO}$*/al2*$^{KO/KO}$ mouse model (Fig S5)
304 phenocopied our previously characterised *Katnal2* mutant models[5], including having a
305 comparable spermiation failure phenotype, sperm head shaping defects (knobby heads), and
306 an absence of normal sperm tail development (Fig S5). No aspect of the infertility phenotype
307 appeared worse that the loss of KATNAL2 in isolation. These data reveal that KATNA1 and
308 KATNAL2 do not have compensatory function in male germ cell development.
309
310 By contrast the removal of KATNA1 and KATNAL1 from germ cells resulted in a significantly
311 worse male fertility phenotype than seen in either individual knockout, especially in meiosis.
312 Successful ablation of both *Katna1* and *Katnal1* from male germ cells was confirmed by qPCR
313 (Fig 4A,B). Test mating of the *Katna1/al1*$^{GCKO/GCKO}$ male mice with wild-type females,

314 revealed loss of both KATNA1 and KATNAL1 from male germ cells results in male sterility
315 (7.1±3.2 SD pups / plug sired by *Katna1/al1*$^{Flox/Flox}$ males versus 0± 0 SD pups / plug sired by
316 *Katna1/al1*$^{GCKO/GCKO}$ males (P=0.0175)). Moreover, assessment of the reproductive tract
317 revealed a 48.5% reduction in testis weight, an 89% reduction in daily sperm output and a
318 96.2% reduction in epididymal sperm content compared to controls (Fig 4D-F). Examination
319 of *Katna1/al1*$^{GCKO/GCKO}$ seminiferous tubule histology instantly revealed large scale germ cell
320 loss during both meiosis and spermiogenesis that was significantly worse than in either single
321 gene deletion (Fig 4G-H). Numerous pyknotic spermatocytes were observed in all stage XII
322 and I *Katna1/al1*$^{GCKO/GCKO}$ tubules indicative of cells stalling in meiosis followed by apoptosis
323 but were rare in *Katna1/al1*$^{Flox/Flox}$ (Fig 4G-H, magenta arrowheads). Of the germ cells that
324 progressed through meiosis in *Katna1/al1*$^{GCKO/GCKO}$, the vast majority became pyknotic by
325 steps 12-13 (stages XII-I) of elongating spermatid development (Fig 4H, green arrowheads)
326 and as a result elongated spermatids were absent past stage II-VIII *Katna1/al1*$^{GCKO/GCKO}$ tubules
327 (Fig 4H). Moreover, analysis of cleaved caspase 3/7 immunolabelling revealed a 6.4 fold
328 increase in the number of apoptotic germ cells in *Katna1/al1*$^{GCKO/GCKO}$ versus
329 *Katna1/al1*$^{Flox/Flox}$ seminiferous tubules (Fig 4O). The majority of apoptotic cells were
330 spermatocytes that had stalled in anaphase I and meiosis II in stage I tubules (Fig 5J,N), and to
331 a lesser degree those undergoing metaphase I in stage XII (Fig 5J,N). In line with these defects,
332 analysis of epididymal sections confirmed almost no sperm reached the *Katna1/al1*$^{GCKO/GCKO}$
333 epididymis. The bulk of the cells in the lumen of *Katna1/al1*$^{GCKO/GCKO}$ epididymides were
334 instead prematurely sloughed round germ cells (Fig 4P, arrowheads).
335
336 Assessment of *Katna1/al1*$^{GCKO/GCKO}$ meiotic spindles, via the immunolabelling of testis
337 sections for α-tubulin, revealed that while meiotic spindles formed in *Katna1/al1*$^{GCKO/GCKO}$
338 spermatocytes, most were morphologically abnormal compared to *Katna1/al1*$^{Flox/Flox}$ controls

339 (Fig 5A,B). At metaphase, in contrast to the tightly packed morphology of *Katna1/al1*$^{Flox/Flox}$
340 controls (Fig 5Aa,Ba,e), chromosomes were loosely dispersed along the metaphase plate in
341 *Katna1/al1*$^{GCKO/GCKO}$ mice (4Bb,f). Misaligned and/or lagging chromosomes were frequently
342 observed in *Katna1/al1*$^{GCKO/GCKO}$ metaphase and anaphase spermatocytes (Fig 5A,B). As
343 detailed above, these defects ultimately lead to a large proportion of *Katna1/al1*$^{GCKO/GCKO}$
344 metaphase and anaphase spermatocytes stalling and undergoing apoptosis in stage XII-I
345 seminiferous tubules (Fig 4H, I-O). Of note, examination of *Katna1/al1*$^{GCKO/GCKO}$ stage I
346 tubules, revealed that these stalled metaphase and anaphase spermatocytes where characterised
347 by the ectopic accumulation of α-tubulin throughout their cytoplasm (Fig 5Ah,i) indicating
348 that KATNA1/KATNAL1-mediated severing restrains MT bulk in spermatocytes. Of the
349 subset of *Katna1/al1*$^{GCKO/GCKO}$ spermatocytes that progressed through meiosis, overtly normal
350 midbody formation was observed in telophase (Fig 5Ag,k). However, indicative of failure of
351 midbody to intracellular bridge conversion and similar to *Katna1*$^{GCKO/GCKO}$ mice, binucleated
352 spermatids were frequently observed in *Katna1/al1*$^{GCKO/GCKO}$ mice but never in
353 *Katna1/al1*$^{Flox/Flox}$ controls (Fig 5Ag,k). Consistent with compromised anaphase chromosome
354 segregation, abnormally large round spermatids were frequent in *Katna1/al1*$^{GCKO/GCKO}$ mice
355 but never in *Katna1/al1*$^{Flox/Flox}$ controls (Fig 5Ag,h). Collectively these data indicate that
356 KATNAL1 and KATNA1 can at least partially compensate for each other in metaphase and
357 anaphase of male meiosis. The frequency of binucleated spermatids in *Katna1/al1*$^{GCKO/GCKO}$
358 mice however, was similar to that of *Katnal1*$^{GCKO/GCKO}$ suggesting KATNA1 does not
359 compensate for KATNAL1 in cytokinesis.
360
361 Assessment of spermiogenesis in *Katna1/al1*$^{GCKO/GCKO}$ mice revealed that unlike the single
362 GCKO mice, acrosome biogenesis was overtly abnormal in the absence of both KATNA1 and
363 KATNAL1 indicating functional compensation between these two A-subunits (Fig 6A,B). In

364 PAS-stained *Katna1/al1*$^{Flox/Flox}$ control testis sections, a single PAS-positive acrosomal vesicle
365 was observed to adhere to step 2-3 round spermatid nuclei (stage II-III) in the Golgi phase of
366 acrosome development, and progressively spread to cover the apical half of the spermatid
367 nuclei as spermiogenesis progressed (Fig 6A). In *Katna1/al1*$^{GCKO/GCKO}$ mice however, a large
368 subset of round spermatids with supernumerary ectopic acrosomal vesicles were observed (Fig
369 6A orange arrowheads), in addition to a smaller subset of round spermatids wherein pro-
370 acrosomal vesicles had failed to attach to the nucleus at the appropriate time (Fig 6A, yellow
371 arrowheads). As spermiogenesis progressed, elongating spermatids with fragmented and
372 partially detached acrosomes were common in *Katna1/al1*$^{GCKO/GCKO}$, but never seen in
373 *Katna1/al1*$^{Flox/Flox}$ controls (Fig 6A, blue arrowheads). Ectopic PAS-positive vesicles were also
374 present throughout the seminiferous epithelium during multiple steps of acrosome biogenesis
375 in *Katna1/al1*$^{GCKO/GCKO}$, but not *Katna1/al1*$^{Flox/Flox}$, mice (Fig 6A, green arrowheads). TEM of
376 acrosome biogenesis confirmed these observations (Fig 6B), and revealed morphological
377 abnormalities in the spermatid Golgi apparatus of *Katna1/al1*$^{GCKO/GCKO}$ mice (Fig 6Bi,k)
378 compared to *Katna1/al1*$^{Flox/Flox}$ mice (Fig 6Bc,e). In normal round spermatids, and as seen in
379 *Katna1/al1*$^{Flox/Flox}$ mice (Fig 6Bc,e), the Golgi apparatus has a flattened sometimes horseshoe-
380 like morphology wherein the trans-Golgi network (TGN) is closely associated with, and
381 oriented in parallel to, the apical nuclear membrane. In *Katna1/al1*$^{GCKO/GCKO}$ mice however the
382 Golgi stacks were disorganised, often displaying a circular morphology, wherein the cis-Golgi
383 network almost entirely enclosed the TGN (Fig 6Bi), or a dispersed, splayed morphology (Fig
384 6Bk). These phenotypes, reveal KATNA1 and KATNAL1 collectively regulate the spatial
385 organisation of the Golgi apparatus and the transport of proacrosomal vesicles, and their fusion,
386 to the nuclear membrane. The acrosome abnormalities observed in *Katna1/al1*$^{GCKO/GCKO}$ mice,
387 are reminiscent of those seen in KATNB1 loss of function mice[11] suggesting these KATNA1
388 and KATNAL1 likely function in complexes with KATNB1 during acrosome biogenesis.

389

390 Analysis of the key MT-based structures required for spermiogenesis revealed phenotypes
391 consistent with a loss of MT severing and global dysregulation of the MT cytoskeleton. Similar
392 to *Katna1*$^{GCKO/GCKO}$ mice, immunolabelling of testis sections for acetylated tubulin revealed
393 sperm tails formed in *Katna1/al1*$^{GCKO/GCKO}$ mice, however reflective of sperm numbers fewer
394 tails were seen than in *Katna1/al1*$^{Flox/Flox}$ controls (Fig 6C-F). Acetylated tubulin staining
395 however, revealed the frequent ectopic accumulation of stable MTs in the cytoplasm of
396 spermatids in *Katna1/al1*$^{GCKO/GCKO}$ mice (Fig 6E-F), consistent with the decreased turnover of
397 MTs.

398

399 Assessment of manchette formation via the immunolabelling of testis sections for α-tubulin
400 revealed a catastrophic dysregulation of manchette formation. MTs accumulated around the
401 spermatid nucleus at stage VIII in *Katna1/al1*$^{GCKO/GCKO}$ mice (Fig 6G), however they failed to
402 assemble into a sheath around, and with MTs aligning in parallel to, the distal half of the
403 nucleus. Instead, the cytoplasm of the elongating spermatids became enriched in ectopic α-
404 tubulin as spermiogenesis progressed (Fig 6G). Analysis of elongating spermatid ultrastructure
405 via TEM confirmed these observations (Fig 6H). In *Katna1/al1*$^{Flox/Flox}$ mouse elongating
406 spermatids, a typical manchette structure wherein MTs projected distally from a perinuclear
407 ring was observed (Fig 6H). In *Katna1/al1*$^{GCKO/GCKO}$ mice, MTs were observed throughout the
408 cytoplasm of elongating spermatids, however these were never associated with a perinuclear
409 ring and were not arranged into typical manchette structure (Fig 6H). Collectively, these results
410 reveal that KATNA1/KATNAL1-mediated severing is required to restrain MT growth/prune
411 MT bulk during spermatid differentiation and to regulate manchette formation. Moreover, the
412 absence of these phenotypes in the single GCKO KATNA1 and KATNAL1 models, suggest
413 KATNA1 and KATNAL1 can compensate for each other in these aspects of spermiogenesis.

414

415 **KATNA1, KATNAL1 and KATNB1 interact with a range of cytoskeletal and vesicular**
416 **transport proteins in the mouse testis**

417 To explore the mechanism of action of KATNA1 and KATNAL1 during male meiosis and
418 spermiogenesis, and how they functionally compensate for each other, we determined the
419 respective interactome for KATNA1, KATNAL1 and KATNB1, within testis
420 immunoprecipitates via MS (Table S1 and Fig S6A-C). A total of 322, 108 and 213 proteins
421 were significantly enriched in the KATNA1, KATNAL1 and KATNB1 IP respectively
422 compared to their corresponding controls (Table S1 and Fig S6A-C). As expected, KATNA1,
423 KATNAL1 and KATNB1 were all significantly enriched in their own IPs validating the
424 specificity of each IP. KATNA1 and KATNAL1 were not found in the binding partner list for
425 each other, suggesting that they do not interact with each other to form heterohexamers (Table
426 S1). Similarly, neither bound to KATNAL2, however KATNAL1 and KATNB1 each pulled
427 the other down (Table S1). Consistent with the three proteins having similar functions, they
428 shared 48 candidate interacting proteins, in addition to 102 candidates that were shared by two
429 katanins (Fig S6D).

430

431 PANTHER protein class and gene ontology analysis[15] was conducted (Table S2 and
432 summarized in Fig S6E-J). Consistent with their regulation of MT-based processes in
433 spermatogenesis, KATNA1, KATNAL1 and KATNB1 each bound several cytoskeletal
434 proteins (Fig S6E-G, Table S2). Of particular relevance to the regulation of the Golgi and
435 acrosome formation all bound proteins involved in vesicle-mediated transport. In addition,
436 KATNA1 bound to known vesicle targeting proteins including ARL3 (Fig S6E-G, Table S2).
437 Functional descriptions of selected cytoskeletal, membrane/vesicle-transport and

438 spermatogenesis related proteins significantly enriched in the KATNA1, KATNAL1 and
439 KATNB1 IP experiments are summarised in Table S3.
440
441 Strikingly, across the three IP experiments the cytoskeletal proteins identified were
442 predominantly actin-related proteins, however tubulin and MT-related proteins were also
443 identified (Fig S6E-J, Table S2 and S3). KATNA1 also bound to the intermediate filament
444 protein vimentin (Table S2 and S3). Of the MT-related proteins identified as katanin testis-
445 interactors, multiple proteins involved in the regulation and activity of dynein MT motor
446 proteins were identified. Indeed, KATNA1 and KATNB1 both bound components of the
447 dynactin complex (Table 1), an essential cytoplasmic-dynein cofactor involved in MT-based
448 cargo transport. KATNA1 also bound DNAAF4, which is required for axonemal dynein
449 assembly and thus ciliary motility, and all three katanins bound NUDC, a dynein-dynactin
450 complex regulator (Table S3). Consistent with the phenotypes of our *Katnb1*[11,12], *Katnal1* and
451 *Katna1/al1* mutant mice, the MT-related proteins identified included those with established
452 functions in the mitotic and/or meiotic spindle (e.g. NUDC, MAPRE1/EB1), intraflagellar
453 transport and ciliogenesis (ARL3) and axoneme assembly DNAAF4; Table S3). Moreover,
454 several have previously been implicated in spermatogenesis and male fertility (e.g. ARL3,
455 DNAAF4, MAPRE1/EB1) and, consistent with its mechanism of action, KATNA1 pulled
456 down both α- and β-tubulin isoforms (Table S3).
457
458 Of the actin-binding proteins identified across the three katanin IP experiments, multiple
459 regulators of actin polymerization/dynamics were identified including components of the
460 ARP2/3 and CapZ complexes (Table S2, S3). KATNA1, KATNAL1 and KATNB1 each bound
461 at least two components of the ARP2/3 complex. Data strongly suggests this complex plays
462 key roles in blood-testis-barrier integrity, spermiogenesis and spermiation[16-19]. Likewise, all

463 bound the CapZ subunit CAPZA1, and KATNA1 and KATNAL1 both bound CAPZA2. In
464 addition, several regulators of actin-network organization were identified to bind KATNA1
465 and KATNB1, and KATNA1 bound MYL6, an actin motor protein which localizes to the
466 manchette (Table S3). Collectively, these data indicate a novel connection between katanin
467 proteins and the actin cytoskeleton in male germ cells. This is consistent with data showing the
468 *Arabidopsis* katanin A-subunit KATANIN1 regulates the actin cytoskeleton[20] and that cortical
469 localisation of *Drosophila* KATNA1 orthologue kat-60 is actin-dependent[21].
470
471 KATNA1 and KATNB1 bound multiple Rab GTPases, a family which regulates multiple
472 aspects of vesicle transport (vesicle budding, actin/MT-mediated transport and fusion) (Tables
473 1, S1 and S2). Of note in spermatogenesis there is increasing evidence Rab and Rab-like
474 proteins mediate pro-acrosomal vesicle transport, in addition to intraflagellar transport and
475 sperm tail development[22-25]. Other transport proteins included those related to endoplasmic
476 reticulum (ER) to Cis-Golgi transport, intra-Golgi transport, clathrin-mediated vesicle
477 disassembly and endocytosis (Table 1). Further consistent with the acrosome defects in
478 *Katna1/al1*$^{GCKO/GCKO}$ mice, KATNAL1 bound ACRBP a protein essential for acrosome granule
479 formation and maintenance of acrosome integrity, and consistent the Golgi defects, a number
480 of proteins were identified with roles in Golgi organization (e.g. Rab2, Rab6, VCP, LMAN1;
481 Table S3).
482
483 Other notable proteins identified as binding the katanins included essential male meiosis
484 regulators TEX15 (KATNA1 IP) and HSPA2 (KATNA1/B1 IP), and FABP9 a protein required
485 for normal sperm head shape in mice (KATNA1/AL1 IP) (Table S3).
486
487 **Discussion**

488 Katanin MT severing enzymes are potent regulators of MT dynamics and organization across
489 eukaryotes. Herein, using a combination of single and double katanin A-subunit GCKO mice,
490 we show for the first time the essential requirement for katanin A-subunits in mammalian male
491 meiosis, provide the first direct evidence that different katanin A-subunits can functionally
492 compensate for one another and establish KATNA1 and KATNAL1 as novel regulators of
493 spermatid differentiation (spermiogenesis). Specifically, KATNA1 and KATNAL1
494 collectively regulate spermatocyte metaphase and anaphase spindle structure and function,
495 acrosome development via the Golgi apparatus and pro-acrosomal vesicle trafficking, sperm
496 head shaping via manchette formation, and collectively restrain MT bulk during male meiosis
497 and spermiogenesis. In addition to this, KATNAL1 regulates spermatocyte cytokinesis, sperm
498 tail and HTCA development, manchette dynamics and dissolution, and the release of sperm
499 from the seminiferous epithelium (spermiation). Through the analysis of KATNA1,
500 KATNAL1, and KATNB1 testis binding proteins, we reveal these activities involve
501 interactions with a diverse suite of proteins, including actin-, MT-, vesicle/membrane
502 trafficking-, and spermatogenesis-related proteins.
503
504 The finding that KATNA1 and KATNAL1, but not KATNA1 and KATNAL2, have gene
505 redundancy in mammalian spermatogenesis is consistent with the highly similar domain
506 structure and severing activity shared between KATNA1 and KATNAL1, but not KATNAL2
507 [2]. Interestingly, KATNAL1 fully compensates for KATNA1 germ cell loss, whereas KATNA1
508 can only partially compensate for germ cell KATNAL1 loss. This suggests KATNAL1 is the
509 more potent/efficient MT severing enzyme in the testis, and/or that it has neofunctionalized to
510 acquire additional functions. We predict it is a combination of the two. Indeed, KATNAL1 has
511 possesses higher MT severing activity in mouse Neuro-2a cells, and is less prone to degradation
512 in HEK293T cells compared to KATNA1[26]. However, we also identified several different

513 KATNA1 versus KATNAL1 testis interacting proteins indicating they have at least some
514 distinct modes of regulation and/or function. These findings have important implications for
515 the study of katanin proteins in contexts wherein multiple A-subunits exist, revealing that
516 discovery of full katanin function can require double KO models.
517
518 We identify KATNA1/KATNAL1 as essential regulators of metaphase and anaphase spindle
519 structure, metaphase chromosome alignment, anaphase chromosome segregation and,
520 KATNAL1 as a cytokinesis regulator during male meiosis. While a role for katanin A-subunits
521 in male mammalian meiosis has never previously been shown, we have previously shown the
522 B-subunit, KATNB1 is essential for normal spindle architecture and function, and for
523 cytokinesis in mouse spermatocytes[11,12]. In strong support of these overlapping functions being
524 due to KATNB1 working in partnership with KATNA1 and KATNAL1, KATNB1-KATNA1
525 and KATNB1-KATNAL1 complexes are present throughout mouse male meiosis wherein they
526 localize to spindle MTs[11]. That single GCKO of KATNAL1, but not KATNA1, is sufficient to
527 cause meiotic defects, agrees with our previous data showing KATNB1-KATNAL1 complexes
528 are the most abundant type of katanin complex during male meiosis[11].
529
530 The misalignment of metaphase chromosomes, followed by uneven anaphase segregation in
531 *Katnal1*$^{GCKO/GCKO}$ and *Katna1/al1*$^{GCKO/GCKO}$ meiosis is consistent with KATNA1/KATNAL1
532 regulating MT-chromosome attachment and/or regulating spindle dynamics via metaphase
533 poleward 'flux' (reviewed by Rogers et al.[27]) and anaphase 'Pacman-flux' (reviewed by Rath
534 and Sharp[28]). While future studies will need to directly test this in meiosis, katanin-mediated
535 MT severing has been shown to directly contribute to metaphase spindle flux in HEK293
536 mitotic cells[29] and Pacman-flux in *Drosophila* mitotic cells[30].

537

538 The role for KATNAL1 in cytokinesis identified herein aligns with evidence that midbody
539 disassembly in mitosis requires MT severing (reviewed by McNally et al.[2] and for additional
540 data see Elad et al.[31]) and our own data, regarding KATNB1 function in mouse male
541 meiosis[11,12]. That only a subset of germ cells fails cytokinesis in the absence of KATNAL1 or
542 KATNB1, suggests that other MT severing enzymes must also be involved in this process.
543 Indeed, we have recently shown the related MT severing enzyme, spastin, also contributes to
544 cytokinesis during male meiosis[32].

545

546 Our data establishes KATNA1 and KATNAL1 as novel regulators of Golgi organisation and
547 pro-acrosomal vesicle trafficking and fusion during acrosome biogenesis. This contributes to
548 an emerging body of evidence that MT-severing enzymes regulate vesicle-based transport in
549 spermiogenesis, as we have recently shown spastin and KATNB1 are also essential for pro-
550 acrosomal vesicle transport and fusion events[11,32]. The contribution of KATNA1/KATNAL1 to
551 these processes may be as simples as a role in pruning the MT tracks along which Golgi
552 membranes are spatially positioned and pro-acrosomal vesicles are delivered. However, the
553 interaction of KATNA1, KATNAL1 and KATNB1 with multiple proteins involved in Golgi
554 organisation and vesicle trafficking suggests a more direct role and raises the possibility MT-
555 severing can modulate cargo-MT interactions.

556

557 We have previously shown KATNAL2 is essential for sperm tail development via basal body
558 -plasma membrane docking and the initiation of spermatid axoneme extension[5]. Here, we show
559 KATNAL1 is also required, but in the subsequent assembly, and potential stability, of axoneme

560 MT doublets, and in mitochondrial sheath and ODF development. Moreover, while KATNAL1
561 is not required for basal body-membrane docking, it is required for HTCA formation/integrity.
562 The precise mechanism of KATNAL1 contribution to these processes remains an outstanding
563 question. One possibility is that KATNAL1-mediated MT severing directly amplifies and
564 regulates MTs for axoneme doublet formation and HTCA fortification. However, the
565 variability in phenotypes (e.g. missing MT doublets in some tails and supernumerary MT
566 doublets in others), is more suggestive of mis-regulated cargo trafficking. Of note, and
567 consistent with the co-incident manchette defects in KATNAL1 loss, sperm tail components
568 including the ODFs, and proteins required to strengthen the HTCA appear to be delivered via
569 the MTs of the manchette, and abnormal sperm tail and manchette phenotypes often occur in
570 parallel (reviewed by Lehti and Sironen[33]). It is thus possible that the abnormal manchette
571 phenotypes in *Katnal1*$^{GCKO/GCKO}$ mice underpin at least some of the sperm tail defects.

572

573 The manchette phenotypes identified in the *Katnal1*$^{GCKO/GCKO}$ mice establish roles for
574 KATNAL1 in manchette migration down the sperm nucleus, which requires 'unzipping' of
575 rod-like manchette-nuclear linkers, and in controlling manchette MT length and in manchette
576 MT disassembly. These functions are consistent with a direct MT-severing mechanism.
577 Strikingly, the *Katnal1*$^{GCKO/GCKO}$ mouse manchette phenotypes, mirror not only those in
578 KATNB1 loss of function mice[11,12], but also those in KATNAL2 loss[5]. These identical yet non-
579 redundant KATNAL1 and KATNAL2 phenotypes suggest the two proteins are executing
580 similar functions in the manchette but severing different MT subpopulations. This is consistent
581 with our proteomics data, demonstrating KATNAL2 is not a binding partner of KATNAL1.

582

583 Similar to the established roles of Sertoli cell KATNAL1 is required to maintain round
584 spermatid-Sertoli cell adhesion[13]. We show germ cell KATNAL1 is involved in spermatid
585 retention and elongated spermatid release via spermiation. Data is consistent with KATNAL1
586 severing the cytoskeletal connections tethering elongating spermatids to the Sertoli cell. The
587 precise cytoskeletal targets of this action need to be identified, but of note, our IP revealed
588 katanins interact with multiple ARP2/3 complex proteins. The ARP2/3 complex appears to
589 facilitate spermiation, *albeit* via the disassembly of the Sertoli cell actin cytoskeleton [19]. Of
590 note spermiation defects in KATNAL2 mutant mice [5], and spermatid adhesion and spermiation
591 defects seen in the KATNB1 mutant mice[11,12] phenocopy those seen in *Katnal1*$^{GCKO/GCKO}$ mice.
592 This suggests that KATNAL1-KATNB1 complexes along with KATNAL2-KATNB1
593 complexes facilitate spermatid release.

594

595 Finally, we defined the testis interactome for KATNA1, KATNAL1 and KATNB1. While a
596 katanin interactome has previously been defined in HELA cells[4], this is the first *in vivo* tissue
597 wide interactome for each protein. A number of protein classes were identified that we predict
598 are related to the activation/inhibition of katanin function (e.g. metabolite interconversion
599 enzymes). Of proteins that we predict are involved specific testis functions of the katanin
600 enzymes, cytoskeletal and vesicle-transport related proteins emerged as key protein classes.
601 Future studies will need to define precise nature of these interactions, however they paint a
602 picture of katanin action involving a complex crosstalk between different cytoskeletal networks
603 notably between actin and MT networks, and suggest a direct role for katanins in regulating
604 the interaction of dynein- and vesicle-based cargo machinery with MTs.

605

606 Collectively, this study establishes KATNA1 and KATNAL1 as novel players in male germ
607 cell MT regulation. The data defined herein, taken together with our previous data on the roles
608 of KATNB1[11,12], KATNAL2[5] and Sertoli cell KATNAL1[13], allows us to define a model of the
609 complete katanin 'toolbox' during mammalian spermatogenesis (Fig 7). This data
610 unequivocally shows the emergence of multiple katanin A-subunits in higher eukaryotes, not
611 only allows for functional sub-specialization and thus customized cutting of discrete MT
612 subpopulations, but also for the protection of katanin function in critical processes such as
613 meiosis through gene redundancy.

614

615

616 **Methods**

617

618 **Mouse model production**

619 All animal procedures were approved by the Monash University School of Biological Sciences
620 Animal Experimentation Ethics Committee and the University of Melbourne Ethics committee
621 and conducted in accordance with National Health and Medical Research Council (NHMRC)
622 Guidelines on Ethics in Animal Experimentation.

623

624 To the generate *Katna1*$^{Flox/Flox}$ mice, *Katna1* KO-first conditional-ready mice (*Katna1*$^{KO/WT}$)
625 were generated through the Monash University Node of the Australian Phenomics Network
626 using a EUCOMM *Katna1* KO-first conditional-ready ES clone (EPD0586_1_B10) as
627 described[34]. To disrupt the *Katna1* gene, the FRT-LacZ-loxP-Neo-FRT-loxP-*Katna1-exons6-*
628 *7*-loxP cassette was inserted into intron 5 of the *Katna1* gene (Fig S1C). To generate
629 conditional *Katna1* mouse (*Katna1*$^{Flox/Flox}$), mice heterozygous for the knockout-first allele
630 (*Katna1*$^{KO/WT}$) were then crossed with a transgenic line carrying the *Flp* recombinase gene.

631 This resulted in removal of the *FRT* flanked gene-trap cassette, exposing a floxed *Katnal1* exon
632 6-7 and reverting mice to a wild-type phenotype. *Katna1*$^{GCKO/GCKO}$ were then generated using
633 a two-step breeding strategy. (1) *Katna1*$^{Flox/Flox}$ females were mated with a *Stra-8-cre*
634 transgenic line to produce *Katna1*$^{WT/Flox,Stra8\text{-}cre+}$ males. (2) *Katna1*$^{WT/Flox,Stra8\text{-}cre+}$ males were
635 mated with *Katna1*$^{Flox/Flox}$ females to produce *Katna1*$^{Flox/Flox,Stra8\text{-}cre+}$ progeny
636 (*Katna1*$^{GCKO/GCKO}$). In these mice, gene disruption relied on Cre-lox recombination mediated
637 excision of *Katna1* exons 6 and 7 (ENSMUSE00001254109, ENSMUSE00001247569), and
638 the *Stra8-Cre* used is expressed from late spermatogonia onwards [35].
639
640 *Katnal1*$^{Flox/Flox}$ mice, wherein exon 3 (ENSMUSE00001360953) of the *Katnal1* gene is flanked
641 by loxP sites, were generated by the Monash Genome Modification Platform using
642 CRISPR/Cas9 technology. Guide RNA target sites flanking the target exon (5' end of exon -
643 5' TCAATGTCTGAGGTGGATAA 3' and 3' end of exon - 5'
644 CAAAGAAGTCTTTTAGACCC 3') were identified using the UCSC Genome Browser. A
645 single stranded DNA homology directed repair template, was generated from a *Katnal1*
646 conditional KO targeting construct using the Guide-it Long ssDNA Strandase Kit (Takara,
647 632645). The following oligonucleotides were used to generate a PCR product from which the
648 ssDNA was generated: 5'/5Biosg/GATGCTTAGCACTGGCTGG 3' and 5'
649 GAACGTGTGCTATTTGGTCTTTAAG 3'. The CRISPR/Cas9 ribonucleoprotein complex
650 and single stranded DNA homology repair templates were microinjected into C57BL/6J
651 zygotes at the pronuclei stage and transferred into the uterus of pseudo-pregnant females.
652 *Katnal1*$^{GCKO/GCKO}$ mice were generated by intercrossing *Katnal1*$^{Flox/Flox}$ mice with a *Stra8-cre*
653 transgenic line as above. *Katnal2*$^{Flox/Flox}$ mice were generated as previously described[5].
654 *Katna1/al1*$^{Flox/Flox}$ and *Katna1/al2*$^{Flox/Flox}$ mice were generated by breeding *Katna1*$^{Flox/Flox}$ mice
655 with either *Katnal1*$^{Flox/Flox}$ or *Katnal2*$^{Flox/Flox}$ mice, respectively. Double germ cell deletion was

656 then achieved using by intercrossing double floxed mice with a *Stra8-cre* transgenic line as
657 above.
658
659 All mice were maintained on a C57BL/6 background. To control for background strain effects
660 on phenotype, *Katna1*$^{Flox/Flox}$, *Katnal1*$^{Flox/Flox}$, *Katna1/al1*$^{Flox/Flox}$ and *Katna1/al2*$^{Flox/Flox}$ mice
661 mice were used as controls for *Katna1*$^{GCKO/GCKO}$, *Katnal1*$^{GCKO/GCKO}$, *Katna1/al1*$^{GCKO/GCKO}$ and
662 *Katna1/al2*$^{GCKO/GCKO}$ mice, respectively. Mouse genotypes were determined from tail biopsies
663 using real time PCR with specific probes designed for each allele (Transnetyx, Cordova, TN).
664 Efficiency of exon excision in *Katna1*$^{GCKO/GCKO}$, *Katnal1*$^{GCKO/GCKO}$, *Katna1/al1*$^{GCKO/GCKO}$ and
665 *Katna1/al2*$^{GCKO/GCKO}$ mice, was determined by qPCR of isolated germ cells as described below.
666 Protein levels were determined by western blotting of germ cell and testis lysates as described
667 below.
668
669 **Quantitative qPCR**
670 Purified germ cells were prepared via the STAPUT method as detailed in [36]. Total RNA was
671 then extracted from purified germ cells using Trizol (Life Technologies), and reverse-
672 transcribed into cDNA using SuperScript III Reverse Transcriptase (Life Technologies).
673 Primers spanning *Katna1* exons 6 and 7 (5'-TCAGGAAGCAGTGGTGTTACC-3' forward
674 and 5'-AAGGGTCTTTCCAGTGCCAG-3' reverse), *Katnal1* exons 3 and 4 5'-
675 CCGTGTCTTGCCGAGATGAA-3'forward and 5'-GCGATTTGGACGCCTGATTT-3'
676 reverse) and *Katnal2* exons 2 and 3 (5'-AAGGCTTTGGAGGAGGAGAC-3' forward and 5'-
677 GGGGCCTTCTTAACCACTTT-3') were used to verify gene deletion in the corresponding
678 mouse models. All qPCRs were performed using SYBR Select Master Mix (Applied
679 Biosystems). Each reaction was performed in triplicate using the Agilent Mx3000P qPCR
680 system or an Applied Biosystems QuantStudio 3 Real-Time PCR System with the parameters

681 of 50°C for 2 minutes, 95°C for 10 minutes followed by 40 cycles of 95°C for 15 seconds and
682 60°C for 1 minute. *Ppia* was amplified at the same time as an internal control (using 5'-
683 CGTCTCCTTCGAGCTGTTT-'3 forward and 5'-CCCTGGCACATGAATCCT-'3 reverse
684 primers), and all results were normalized to *Ppia* expression. Differential expression was
685 analysed using the $2\Delta\Delta^{CT}$ method[37].
686
687 **Male fertility characterisation**
688 Male fertility of all mouse models was characterised as per[38]. Male fertility was assessed by
689 mating 10-12 week old males with wild-type females (≥6 weeks of age). Copulatory plugs
690 were monitored to confirm successful mating and the number of pups born per copulatory plug
691 was recorded. Each male was test mated with 2-3 females and pup numbers averaged. Testis
692 daily sperm production (DSP) and total epidydimal sperm content were determined using the
693 Triton X-100 solubilisation method[39] (n≥3/genotype) as modified in[11]. To assess sperm
694 motility, sperm were backflushed as per[40] from cauda epididymides and motility was assessed
695 using a computer assisted sperm analyser, as described previously[41].
696
697 For histology, testis and epididymal tissue were fixed in Bouin's fixative and histology
698 assessed using standard methods. Male reproductive tract histology was visualised using
699 periodic acid-Schiff's (PAS) and haematoxylin staining, and air-dried caudal epididymal sperm
700 smears were visualised using haematoxylin and eosin staining (n≥3/genotype). Germ cell
701 apoptosis was evaluated by immunostaining for cleaved Caspase 3 and 7 as per[42] and as
702 described below. The number of Caspase-positive cells in a minimum of 50 randomly selected
703 seminiferous tubules per mouse were counted and statistical analysis conducted as described
704 below and as per[11](n≥3 mice /genotype).
705

706 **TEM**

707 For analysis of seminiferous tubule ultrastructure, partially decapsulated testes and cauda
708 epididymides were fixed with 5% glutaraldehyde/4% paraformaldehyde/0.02% picric acid in
709 0.1 M sodium cacodylate buffer, pH 7.4. as per[11]. Samples were *en bloc* stained with 2% uranyl
710 acetate and all samples were embedded into Epon resin using standard procedures. Ultrathin
711 sections were cut on a Leica EM UC7 Ultramicrotome and placed on Copper 100×100 square
712 grids (ProSciTech). Sections were analysed using a FEI Talos L120CI TEM in the Ian Holmes
713 Imaging Centre (The University of Melbourne, Parkville)

714

715 **Antibody use**

716 Primary antibodies used included those against acetylated-tubulin (T6793, Sigma, RRID:
717 Ab_477585, ascites fluid, 1 in 10,000), α-tubulin (T5168, Sigma, ascites fluid, 1 in 50,000),
718 cleaved-Caspase 3 (9664, Cell Signalling, 0.5 μg ml^{-1}), cleaved-Caspase 7 (9491, Cell
719 Signalling, 0.23 μg ml^{-1}), KATNA1 (as described previously [11]), KATNAL1 (as described
720 previously[11]), KATNB1 (as described in [11]), SUN5 (ProteinTech 17495-1-AP 0.8 μg/ml) and
721 TUBB3 (Sigma-Aldrich, SAB3300047, 0.15 μg ml^{-1}). Secondary antibodies included Alexa
722 Fluor 488 donkey anti-mouse (A212062 Invitrogen), Alexa Fluor 488 donkey anti-rabbit
723 (A21206, Invitrogen), and Alex Fluor 555 donkey anti-rabbit (A31572, Invitrogen). EnVision+
724 Dual Link System-HRP (K4063, Dako) was used to amplify signal. The specificity of
725 immunolabelling was determined by staining sections in parallel in the absence of primary
726 antibody or where available KO mouse tissue.

727

728 **Western blotting**

729 Proteins were extracted from STAPUT purified germ cells [36], and immunoblotting conducted
730 as previously described[36]. Images were captured using a ChemiDoc MP Imaging System

731 (BioRad). The molecular weights of detected proteins were estimated using a PageRuler Plus
732 Prestained Protein Ladder (ThermoFisher) and the Image Lab 6.0 Molecular Weight Analysis
733 Tool (BioRad).
734
735 **Immunochemistry and imaging**
736 To assess KATNA1 testis localisation, 5 μm cryostat testis sections were fixed in 1:1 methanol-
737 acetone and permeabilised in 0.2% Triton X-100 in PBS as per[43]. To assess testis localisation
738 of all other proteins, Bouin's fixed testes were processed into paraffin and 5 μm sections
739 prepared using standard methods. Paraffin sections were dewaxed and heat-mediated antigen
740 retrieval was conducted by microwaving sections 10 mM citrate buffer (pH 6) for 16 minutes
741 as per [44]. For sections to be used for chromogenic immunohistochemistry (α-tubulin,
742 acetylated-tubulin, cleaved-caspase 3 and 7), endogenous peroxidase activity was then blocked
743 via incubation with 5% H_2O_2 for 5 minutes. For all testis immunolabelling, non-specific protein
744 binding was minimised by incubation with CAS-block (Invitrogen) for 30 minutes and sections
745 were then incubated with primary antibodies diluted in DAKO Antibody Diluent overnight at
746 4°C. For immunofluorescent labelling, sections were incubated with the appropriate Alexa
747 Fluor secondary antibodies diluted 1in 500 for 1 hour at room temperature. DNA was then
748 visualised using 1 μg ml^{-1} 4',6-diamidino-2-phenylindole (DAPI, Invitrogen) or 4 μM TO-
749 PRO-3 Iodide (TOPRO, Thermo Scientific). Acrosomes were visualized using 0.5 μg ml^{-1}
750 lectin peanut agglutinin (PNA), Alexa Fluor 488 conjugate (L21409, Life Technologies). For
751 chromogenic immunohistochemistry, sections were incubated with DAKO EnVision+ Dual
752 Link System-HRP for 30 minutes at room temperature. The Liquid DAB+ Substrate
753 Chromogen System (DAKO, K3468) was then applied as per the manufacturer's instructions.
754 Nuclei were counterstained using Mayer's haematoxylin (Amber Scientific), followed by
755 Scott's tap water (Amber Scientific).

756

757 To assess SUN5 localisation in cauda epididymal sperm, sperm were washed in PBS and
758 airdried onto slides. Sperm were then fixed in 4% paraformaldehyde for 10 minutes. Sperm
759 were then permeabilised, blocked for non-specific protein binding and immunofluorescently
760 labelled as above.

761

762 Immunofluorescent images were collected using a Leica TCS SP8 confocal microscope (Leica
763 Microsystems) at the Monash Micro Imaging (Monash University) and the University of
764 Melbourne Biological Optical Microscopy Unit (University of Melbourne, Parkville). A
765 63x/1.40 HC PL APO CS2 oil immersion objective was used to take all immunofluorescent
766 images. Bright field images were collected cellSens Imaging Software (Olympus) on an
767 Olympus BX53 light microscope equipped with an Olympus DP80 camera.

768

769 **IP-MS**

770 For IP assays, wild-type mouse testes (n=3 per IP assay) were lysed in 1% NP-40 (PBS)
771 supplemented with protease inhibitor cocktail (Calbiochem, 539134). KATNA1, KATNAL1
772 and KATNB1 and their binding partners were then co-immunoprecipitated using the Pierce
773 Co-immunoprecipitation Kit (Thermo Scientific, 26149) as per the manufacturer's instructions,
774 in combination with either our KATNA1 (10µg per IP column), KATNAL1 (5µg) or KATNB1
775 (5µg) inhouse antibody. Briefly, to reduce non-specific binding, testis protein lysates were first
776 pre-cleared by incubation with 400µl of Pierce control agarose resin slurry for a 0.5-1 hour at
777 4°C with gently rocking. For each pre-cleared testis lysate, 5 mg was then loaded into two IP
778 columns, one which contained the target antibody covalently coupled to the amine reactive
779 Pierce AminoLink Plus Coupling Resin and one which contained the target antibody and a
780 non-amine reactive Pierce Control Agarose Resin (negative control), and incubated overnight

781 at 4°C. Lysate flow through was removed, columns were washed and bound protein eluted and
782 collected as per the manufacturer's instructions. The eluted proteins were neutralised with
783 1.5M Tris-HCL (pH 8.8), reduced with TCEP, then digested by incubation with trypsin
784 overnight at 37°C. Peptide samples were freeze dried and resuspended in 2% acetonitrile
785 (ACN)/0.1% formic acid (FA) (diluted in MilliQ water) before concentrated FA was added to
786 adjust the pH to <3. Samples were purified using reverse-phase chromatography C18 stage
787 tips, which aim to desalt and fractionate in-solution peptides at an acidic pH. The tips were
788 initially activated with 100% methanol and equilibrated with 0.1% FA, before samples were
789 loaded into them and desalted with 0.1% FA. Peptides were eluted with 80% ACN/0.1% FA,
790 freeze dried, resuspended in 2% ACN/0.1% FA and sonicated for 15 minutes in a water bath.

791 The purified peptide samples were analysed via nano liquid chromatography coupled to tandem
792 mass spectrometry (LC-MS/MS). Briefly, the KATNA1 IP and KATNB1 IP samples were
793 analysed at the Monash Proteomics and Metabolomics Facility (Monash University) using an
794 Orbitrap Fusion Tribrid mass spectrometer (ThermoFisher, USA) and a Q-Exactive Hybrid
795 Quadrupole - Orbitrap mass spectrometer (ThermoFisher, USA), respectively. Both
796 instruments were coupled to an UltiMate 3000 RSLCnano system (ThermoFisher, USA)
797 equipped with an Acclaim PepMap RSLC C18 nanoViper Analytical Column (100Å, 75 µm
798 X 50 cm, 2 µm; ThermoFisher, USA) and an Acclaim PepMap 100 C18 HPLC nanoViper Trap
799 Column (100Å, 100 µm X 2 cm, 5 µm; ThermoFisher, USA). The tryptic peptides were
800 separated by increasing concentrations of 80% acetonitrile (ACN) / 0.1% formic acid at a flow
801 rate of 250 nl/min for 128 min and 158 min, respectively. Both mass spectrometers were
802 operated in data-dependent acquisition (DDA) mode to automatically switch between full scan
803 MS and MS/MS acquisition. Each survey full scan (m/z 375–1800) in the Orbitrap Fusion
804 Tribrid acquisitions was acquired in the Orbitrap with 120,000 resolution (at m/z 200) after
805 accumulating ions to a Normalised AGC Target of 250% with a maximum injection time of 54

806 ms. Dynamic exclusion was set to 15 seconds. Adhering to a 2 sec cycle time, the most intense
807 multiply charged ions ($z \geq 2$) were sequentially isolated and fragmented in the collision cell by
808 higher-energy collisional dissociation (HCD) and ms2 scans were acquired with a fixed
809 injection time of 54 ms, 30,000 resolution and a Normalised AGC Target of 400%. Very similar
810 parameters were used for the Q-Exactive Hybrid Quadrupole – Orbitrap acquisitions.

811 The KATNAL1 IP purified peptide samples were analysed at the University of Melbourne
812 Mass Spectrometry and Proteomics Facility, using an Orbitrap Eclipse Tribrid Mass
813 Spectrometer (ThermoFisher, USA) equipped with a nano ESI interface coupled to an Ultimate
814 3000 nano HPLC (Thermo Fisher, USA). The LC system was equipped with an Acclaim
815 Pepmap 100 C18 HPLC nanoViper Trap Column (100 Å, 75 µm X 2 cm, 3 µm; ThermoFisher,
816 USA) and an analytical column as above. The enrichment column was injected with the tryptic
817 peptides (1 µL, 100 ng) at an isocratic flow of 5 µL/min of 2% *v/v* CH_3CN containing 0.05%
818 *v/v* trifluoroacetic acid for 6 min, applied before the enrichment column was switched in-line
819 with the analytical column. The eluents were 0.1% v/v formic acid (solvent A) in H_2O and
820 100% *v/v* CH_3CN in 0.1% *v/v* formic acid (solvent B). The gradient was at 300 nl min^{-1} from
821 (i) 0–6 min, 3 % B; (ii) 6–35 min, 3–23 % B; (iii) 35-45 min, 23-40 % B; (iv) 45-50 min, 40-
822 80 % B; (v) 50-55 min, 80–80 % B; (vi) 55-55.1 min, 80-3 % B; (vii) 55.1-65 min, 3-3 % B.
823 The Eclipse Orbitrap mass spectrometer was operated in the data-dependent mode, wherein
824 full MS^1 spectra were acquired in a positive mode over the range of *m/z* 375-1500, with spray
825 voltage at 1.9kV, source temperature at 275 °C, MS^1 at 120,000 resolution, normalized AGC
826 target of 100 % and maximum IT time of 22 ms. The top 3 second method was used and
827 selecting peptide ions with charge states of ≥ 2-7 and intensity thresholds of ≥ 5E4 were
828 isolated for MS/MS. The isolation window was set at 1.6 *m/z*, and precursors were fragmented
829 using higher energy C-trap dissociation (HCD) at a normalised collision energy of 30, a
830 resolution of 15,000, a normalized AGC target of 100% and automated IT time.

The raw MS data were analysed with the MaxQuant software suite for the identification and quantification of peptides/proteins from the Mouse SwissProt database. Fixed modifications of carbamidomethylation of cysteine as well as variable oxidation of methionine and protein N-terminal acetylation were considered. Trypsin/P was set as the protease with a maximum of 2 missed cleavages. Statistical analysis was conducted with the Perseus software considering protein and PSM false discovery rates (FDR) both set at < 0.01. For each IP assay, the majority UniProt ID(s) for each significantly enriched protein group were then analysed using PANTHER Gene Ontology and protein classification[15]. All MS proteomics data have been deposited to the ProteomeXchange Consortium via the PRIDE partner repository with the dataset identifier PXD038404 [45].

Statistics

Statistical analysis of germ cell apoptosis data was conducted in R version 3.5.1[46]. Generalised linear mixed (GLM) models were used to compare the number of caspase-positive cells per tubule across genotypes, with animal ID included as a random effect to account for repeated measures per individual. For each model, Akaike information criteria (AIC) estimates were used to select the most appropriate error distribution and link function (i.e. poisson, negative binomial, zero-inflated poisson, zero-inflated negative binomial) using the glmer function (lme4 package[47]) and glmmTMB function (glmmTMB, package[48]). For all models, a zero-inflated negative binomial distribution (fitted with glmmTMB, using the ziformula argument) was selected as the most appropriate error distribution and link function (i.e. had the lowest AIC score).

854 All other statistical analysis, other than for the proteomics (described above), was conducted
855 in Graphpad Prism 9.0. The statistical significance of differences between two groups was
856 determined with an unpaired Student t-test. Significance was defined as a P value of <0.05.
857

858 **Acknowledgements**

859 We thank Dr Liza O'Donnell and Dr Duangporn Jamsai for advice on the initial stages of the
860 project. We thank Ms G. Gemma Stathatos, Ms Lauren Rogers and Ms Georgia Shering for
861 technical assistance. We thank Associate Professor Nicholas Williamson, Dr Ching-Seng Ang
862 and Dr Michael Leeming for technical assistance and advice regarding the MS analysis. We
863 thank the following platforms for the use of their facilities and services: at The University of
864 Melbourne (Parkville), the Biological Optical Imaging Platform, the Ian Holmes Imaging
865 Centre, the Mass Spectrometry and Proteomics Facility, the Melbourne Bioresources Platform
866 and the Melbourne Histology Platform; and at Monash University (Clayton), the Monash
867 Animal Research Platform, the Monash Gene Modification Platform, the Monash Histology
868 Platform, Monash Micro Imaging and the Monash Proteomic and Metabolomic Facility.
869

870 **Author Contributions**

871 Conceptualisation, J.E.M.D, M.K.O; Methodology, J.E.M.D, A.E.O, D.J.M, R.B.S, B.J.H and
872 M.K.O; Formal Analysis, J.E.M.D, M.G, K.W, A.E.O, D.J.M, J.N, R.B.S, B.J.H, M.K.O;
873 Investigation, J.E.M.D, M.G, K.W, A.E.O, D.J.M, J.N, R.B.S, B.J.H; Writing – Original Draft,
874 J.E.M.D, M.G, M.K.O; Writing – Review & Editing, J.E.M.D, R.B.S, M.K.O; Visualisation,
875 J.E.M.D, M.G, K.W; Supervision, J.E.M.D, M.K.O; Project Administration, J.E.M.D, M.K.O;
876 Funding Acquisition, M.K.O
877

878 **Declaration of interests**

879 The authors declare no competing or financial interests.

880

881 **Funding**

882 J.E.M.D is supported by a National Health and Medical Research Council Ideas Grant to
883 M.K.O and J.E.M.D (APP1180929) and this project was supported in part by funding from the
884 National Health and Medical Research Council of Australia (APP1138014) and the Australian
885 Research Council (DP160100647). B.J.H is supported by funding from the Male Contraceptive
886 Initiative Fellowship.

887

888 **References**

889 1. Mains, P.E., Kemphues, K., Sprunger, S.A., Sulston, I., and Wood, W. (1990).
890 Mutations affecting the meiotic and mitotic divisions of the early Caenorhabditis
891 elegans embryo. Genetics *126*, 593-605.

892 2. McNally, F.J., and Roll-Mecak, A. (2018). Microtubule-severing enzymes: From
893 cellular functions to molecular mechanism. Journal of Cell Biology *217*, 4057-4069.

894 3. Sarbanes, S.L., Zehr, E.A., and Roll-Mecak, A. (2022). Microtubule-severing enzymes.
895 Current Biology *32*, R992-R997.

896 4. Cheung, K., Senese, S., Kuang, J., Bui, N., Ongpipattanakul, C., Gholkar, A., Cohn,
897 W., Capri, J., Whitelegge, J.P., and Torres, J.Z. (2016). Proteomic analysis of the
898 mammalian katanin family of microtubule-severing enzymes defines katanin p80
899 subunit B-like 1 (KATNBL1) as a regulator of mammalian katanin microtubule-
900 severing. Molecular & Cellular Proteomics *15*, 1658-1669.

901 5. Dunleavy, J.E., Okuda, H., O'Connor, A.E., Merriner, D.J., O'Donnell, L., Jamsai, D.,
902 Bergmann, M., and O'Bryan, M.K. (2017). Katanin-like 2 (KATNAL2) functions in

903 multiple aspects of haploid male germ cell development in the mouse. PLOS Genetics
904 *13*, e1007078.
905 6. Sharp, D.J., and Ross, J.L. (2012). Microtubule-severing enzymes at the cutting edge.
906 Journal of Cell Science *125*, 2561-2569. 10.1242/jcs.101139.
907 7. Gomes, J.-E., Tavernier, N., Richaudeau, B., Formstecher, E., Boulin, T., Mains, P.E.,
908 Dumont, J., and Pintard, L. (2013). Microtubule severing by the katanin complex is
909 activated by PPFR-1–dependent MEI-1 dephosphorylation. Journal of Cell Biology
910 *202*, 431-439. 10.1083/jcb.201304174.
911 8. Loughlin, R., Wilbur, J.D., McNally, F.J., Nédélec, F.J., and Heald, R. (2011). Katanin
912 contributes to interspecies spindle length scaling in Xenopus. Cell *147*, 1397-1407.
913 9. Gao, L.L., Xu, F., Jin, Z., Ying, X.Y., and Liu, J.W. (2019). Microtubule-severing
914 protein Katanin p60 ATPase-containing subunit A-like 1 is involved in pole-based
915 spindle organization during mouse oocyte meiosis. Molecular Medicine Reports *20*,
916 3573-3582.
917 10. Lynn, N.A., Martinez, E., Nguyen, H., and Torres, J.Z. (2021). The mammalian family
918 of katanin microtubule-severing enzymes. Frontiers in Cell and Developmental
919 Biology *9*.
920 11. Dunleavy, J.E.M., O'Connor, A.E., Okuda, H., Merriner, D.J., and O'Bryan, M.K.
921 (2021). KATNB1 is a master regulator of multiple katanin enzymes in male meiosis
922 and haploid germ cell development. Development *148*, dev199922.
923 12. O'Donnell, L., Rhodes, D., Smith, S.J., Merriner, D.J., Clark, B.J., Borg, C., Whittle,
924 B., O'Connor, A.E., Smith, L.B., and McNally, F.J. (2012). An essential role for katanin
925 p80 and microtubule severing in male gamete production. PLOS Genetics *8*, e1002698.
926 13. Smith, L.B., Milne, L., Nelson, N., Eddie, S., Brown, P., Atanassova, N., O'Bryan,
927 M.K., O'Donnell, L., Rhodes, D., and Wells, S. (2012). KATNAL1 regulation of Sertoli

928 cell microtubule dynamics is essential for spermiogenesis and male fertility. PLOS
929 Genetics *8*, e1002697.
930 14. Pleuger, C., Lehti, M.S., Dunleavy, J.E., Fietz, D., and O'Bryan, M.K. (2020). Haploid
931 male germ cells—the Grand Central Station of protein transport. Human Reproduction
932 Update *26*, 474-500. 10.1093/humupd/dmaa004.
933 15. Thomas, P.D., Ebert, D., Muruganujan, A., Mushayahama, T., Albou, L.-P., and Mi,
934 H. (2022). PANTHER: Making genome-scale phylogenetics accessible to all. Protein
935 Science *31*, 8-22. https://doi.org/10.1002/pro.4218.
936 16. Liu, L., Zhang, Y., Chang, X., Li, R., Wu, C., Tang, L., and Zhou, Z. (2018).
937 Fluorochloridone perturbs blood-testis barrier/Sertoli cell barrier function through
938 Arp3-mediated F-actin disruption. Toxicology Letters *295*, 277-287.
939 https://doi.org/10.1016/j.toxlet.2018.07.001.
940 17. Lie, P.P., Chan, A.Y., Mruk, D.D., Lee, W.M., and Cheng, C.Y. (2010). Restricted
941 Arp3 expression in the testis prevents blood–testis barrier disruption during junction
942 restructuring at spermatogenesis. Proceedings of the National Academy of Sciences
943 *107*, 11411-11416.
944 18. Li, N., Mruk, D.D., Tang, E.I., Wong, C.K.C., Lee, W.M., Silvestrini, B., and Cheng,
945 C.Y. (2015). Formins: Actin nucleators that regulate cytoskeletal dynamics during
946 spermatogenesis. Spermatogenesis *5*, e1066476. 10.1080/21565562.2015.1066476.
947 19. O'Donnell, L., Nicholls, P.K., O'Bryan, M.K., McLachlan, R.I., and Stanton, P.G.
948 (2011). Spermiation: the process of sperm release. Spermatogenesis *1*, 14-35.
949 20. Takáč, T., Šamajová, O., Pechan, T., Luptovčiak, I., and Šamaj, J. (2017). Feedback
950 microtubule control and microtubule-actin cross-talk in Arabidopsis revealed by
951 integrative proteomic and cell biology analysis of KATANIN 1 mutants. Molecular &
952 Cellular Proteomics *16*, 1591-1609.

953 21. Zhang, D., Grode, K.D., Stewman, S.F., Diaz-Valencia, J.D., Liebling, E., Rath, U.,
954 Riera, T., Currie, J.D., Buster, D.W., Asenjo, A.B., et al. (2011). Drosophila katanin is
955 a microtubule depolymerase that regulates cortical-microtubule plus-end interactions
956 and cell migration. Nature Cell Biology *13*, 361-369. 10.1038/ncb2206.
957 22. Ramalho-Santos, J., Moreno, R.D., Wessel, G.M., Chan, E.K.L., and Schatten, G.
958 (2001). Membrane Trafficking Machinery Components Associated with the
959 Mammalian Acrosome during Spermiogenesis. Experimental Cell Research *267*, 45-
960 60. https://doi.org/10.1006/excr.2000.5119.
961 23. Shan, M.-M., and Sun, S.-C. (2021). The multiple roles of RAB GTPases in female and
962 male meiosis. Human Reproduction Update *27*, 1013-1029.
963 10.1093/humupd/dmab019.
964 24. Blacque, O.E., Scheidel, N., and Kuhns, S. (2018). Rab GTPases in cilium formation
965 and function. Small GTPases *9*, 76-94.
966 25. Lo, J.C., Jamsai, D., O'Connor, A.E., Borg, C., Clark, B.J., Whisstock, J.C., Field,
967 M.C., Adams, V., Ishikawa, T., and Aitken, R.J. (2012). RAB-like 2 has an essential
968 role in male fertility, sperm intra-flagellar transport, and tail assembly.
969 26. Hatakeyama, E., and Hayashi, K. (2018). KATNAL1 is a more active and stable
970 isoform of katanin, and is expressed dominantly in neurons. Biochemical and
971 biophysical research communications *507*, 389-394.
972 27. Rogers, G.C., Rogers, S.L., and Sharp, D.J. (2005). Spindle microtubules in flux.
973 Journal of Cell Science *118*, 1105-1116.
974 28. Rath, U., and Sharp, D.J. (2011). The molecular basis of anaphase A in animal cells.
975 Chromosome Research *19*, 423-432. 10.1007/s10577-011-9199-2.
976 29. Jiang, K., Rezabkova, L., Hua, S., Liu, Q., Capitani, G., Altelaar, A., Heck, A.J.,
977 Kammerer, R.A., Steinmetz, M.O., and Akhmanova, A. (2017). Microtubule minus-

978 end regulation at spindle poles by an ASPM–katanin complex. Nature cell biology *19*,
979 480-492.
980 30. Zhang, D., Rogers, G.C., Buster, D.W., and Sharp, D.J. (2007). Three microtubule
981 severing enzymes contribute to the "Pacman-flux" machinery that moves
982 chromosomes. The Journal of cell biology *177*, 231-242.
983 31. Elad, N., Abramovitch, S., Sabanay, H., and Medalia, O. (2011). Microtubule
984 organization in the final stages of cytokinesis as revealed by cryo-electron tomography.
985 Journal of Cell Science *124*, 207-215. 10.1242/jcs.073486.
986 32. Cheers, S.R., O'Connor, A.E., Johnson, T.K., Merriner, D.J., O'Bryan, M.K., and
987 Dunleavy, J.E. (2022). Spastin is an essential regulator of male meiosis, acrosome
988 formation, manchette structure and nuclear integrity. bioRxiv.
989 33. Lehti, M., and Sironen, A. (2016). Formation and function of the manchette and
990 flagellum during spermatogenesis. Reproduction *151*, R43-54.
991 34. Cotton, L.M., Meilak, M.L., Templeton, T., Gonzales, J.G., Nenci, A., Cooney, M.,
992 Truman, D., Rodda, F., Lynas, A., and Viney, E. (2015). Utilising the resources of the
993 International Knockout Mouse Consortium: the Australian experience. Mammalian
994 Genome *26*, 142-153.
995 35. Sadate-Ngatchou, P.I., Payne, C.J., Dearth, A.T., and Braun, R.E. (2008). Cre
996 recombinase activity specific to postnatal, premeiotic male germ cells in transgenic
997 mice. Genesis *46*, 738-742.
998 36. Dunleavy, J.E.M., O'Connor, A.E., and O'Bryan, M.K. (2019). An optimised STAPUT
999 method for the purification of mouse spermatocyte and spermatid populations.
1000 Molecular Human Reproduction *25*, 675-683. 10.1093/molehr/gaz056.
1001 37. Livak, K.J., and Schmittgen, T.D. (2001). Analysis of Relative Gene Expression Data
1002 Using Real-Time Quantitative PCR and the $2^{-\Delta\Delta CT}$ Method. Methods *25*, 402-408.

1003 38. Houston, B.J., Conrad, D.F., and O'Bryan, M.K. (2020). A framework for high-
1004 resolution phenotyping of candidate male infertility mutants: from human to mouse.
1005 Human Genetics, 1-28.
1006 39. Cotton, L., Gibbs, G.M., Sanchez-Partida, L.G., Morrison, J.R., de Kretser, D.M., and
1007 O'Bryan, M.K. (2006). FGFR-1 signaling is involved in spermiogenesis and sperm
1008 capacitation. Journal of Cell Science *119*, 75-84.
1009 40. Baker, M.A., Hetherington, L., Weinberg, A., and Velkov, T. (2014). Phosphopeptide
1010 analysis of rodent epididymal spermatozoa. JoVE (Journal of Visualized Experiments),
1011 e51546.
1012 41. Gibbs, G.M., Orta, G., Reddy, T., Koppers, A.J., Martínez-López, P., Luis de la Vega-
1013 Beltran, J., Lo, J.C., Veldhuis, N., Jamsai, D., and McIntyre, P. (2011). Cysteine-rich
1014 secretory protein 4 is an inhibitor of transient receptor potential M8 with a role in
1015 establishing sperm function. Proceedings of the National Academy of Sciences *108*,
1016 7034-7039.
1017 42. O'Bryan, M.K., Clark, B.J., McLaughlin, E.A., D'Sylva, R.J., O'Donnell, L., Wilce,
1018 J.A., Sutherland, J., O'Connor, A.E., Whittle, B., and Goodnow, C.C. (2013). RBM5 is
1019 a male germ cell splicing factor and is required for spermatid differentiation and male
1020 fertility. PLoS genetics *9*, e1003628.
1021 43. Gibbs, G.M., Lo, J.C.Y., Nixon, B., Jamsai, D., O'Connor, A.E., Rijal, S., Sanchez-
1022 Partida, L.G., Hearn, M.T.W., Bianco, D.M., and O'Bryan, M.K. (2010). Glioma
1023 Pathogenesis-Related 1-Like 1 Is Testis Enriched, Dynamically Modified, and
1024 Redistributed during Male Germ Cell Maturation and Has a Potential Role in Sperm-
1025 Oocyte Binding. Endocrinology *151*, 2331-2342. 10.1210/en.2009-1255.
1026 44. Jamsai, D., Bianco, D.M., Smith, S.J., Merriner, D.J., Ly-Huynh, J.D., Herlihy, A.,
1027 Niranjan, B., Gibbs, G.M., and O'Bryan, M.K. (2008). Characterization of

1028 gametogenetin 1 (GGN1) and its potential role in male fertility through the interaction
1029 with the ion channel regulator, cysteine-rich secretory protein 2 (CRISP2) in the sperm
1030 tail. Reproduction *135*, 751-760.
1031 45. Perez-Riverol, Y., Bai, J., Bandla, C., García-Seisdedos, D., Hewapathirana, S.,
1032 Kamatchinathan, S., Kundu, Deepti J., Prakash, A., Frericks-Zipper, A., Eisenacher,
1033 M., et al. (2021). The PRIDE database resources in 2022: a hub for mass spectrometry-
1034 based proteomics evidences. Nucleic Acids Research *50*, D543-D552.
1035 10.1093/nar/gkab1038.
1036 46. R Core Development Team (2015). R: A language and environment for statistical
1037 computing. R Foundation for Statistical Computing.
1038 47. Bates, D., Mächler, M., Bolker, B., and Walker, S. (2015). Fitting Linear Mixed-Effects
1039 Models Using lme4. Journal of Statistical Software *67*. 10.18637/jss.v067.i01.
1040 48. Brooks, M.E., Kristensen, K., van Benthem, K.J., Magnusson, A., Berg, C.W., Nielsen,
1041 A., Skaug, H.J., Machler, M., and Bolker, B.M. (2017). glmmTMB balances speed and
1042 flexibility among packages for zero-inflated generalized linear mixed modeling. The R
1043 Journal *9*, 378-400.
1044
1045

1046 **Figures**

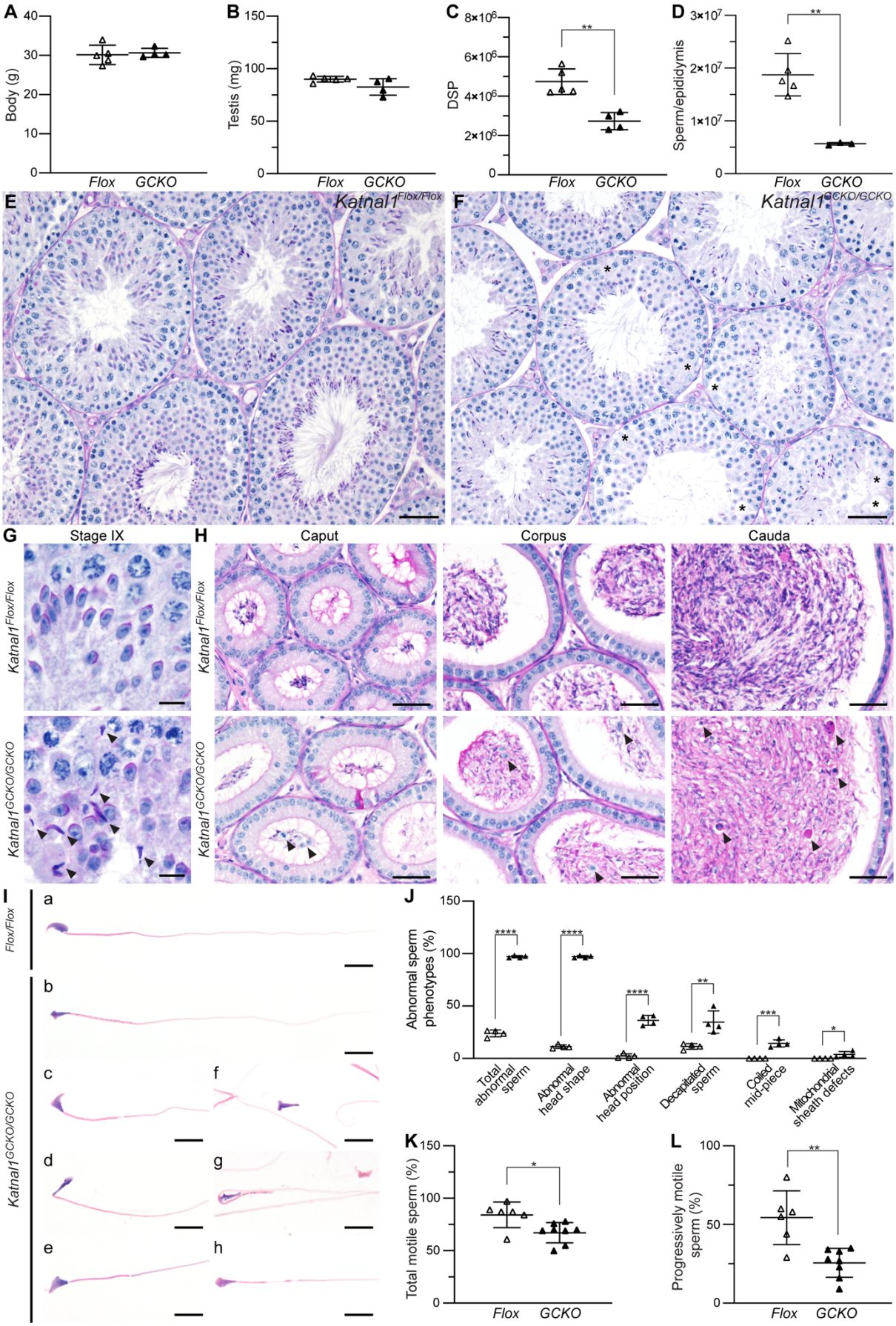

1047

1048 **Figure 1: Germ cell derived KATNAL1 is required for optimal male fertility**

1049 Body weight (**A**), testis weight (**B**), DSP (**C**), and epididymal sperm content (**D**) in
1050 *Katnal1*$^{GCKO/GCKO}$ mice (black triangles) and *Katnal1*$^{Flox/Flox}$ controls (white triangles)
1051 (n≥3/genotype). Lines represent mean ± SD. PAS-stained testis (**E-G**) and epididymis (**H**)
1052 sections. Asterisks indicate areas of seminiferous epithelium with vacuoles or devoid of germ
1053 cells. Black arrowheads indicate retained spermatids. (**I)** Hematoxylin and eosin-stained cauda
1054 epididymal sperm. Abnormalities were observed in the vast majority of sperm from
1055 *Katnal1*$^{GCKO/GCKO}$ mice. Defects included abnormal sperm head shapes - "knobby" (b) and
1056 "hammer" head (c, f), abnormal head sperm head position (d), decapitated sperm (e,), coiled
1057 mid-pieces (g) and occasionally, mitochondrial sheath defects (h). (**J**) Quantification of
1058 abnormal cauda epididymal sperm phenotypes in *Katnal1*$^{Flox/Flox}$ (white triangles) versus
1059 *Katnal1*$^{GCKO/GCKO}$ (black triangles). (n≥3/genotype). Percentage of motile sperm (**K**) and
1060 percentage of progressively motile sperm (**L**) from *Katnal1*$^{Flox/Flox}$ (white triangles) versus
1061 *Katnal1*$^{GCKO/GCKO}$ (black triangles) males. Scale bars in **E-F** = 50 μm**, G** = 10 μm, **H** = 40 μm,
1062 **I** = 10 μm. **P*<0.05 , ***P*<0.01, ****P*<0.01, *****P*<0.001.

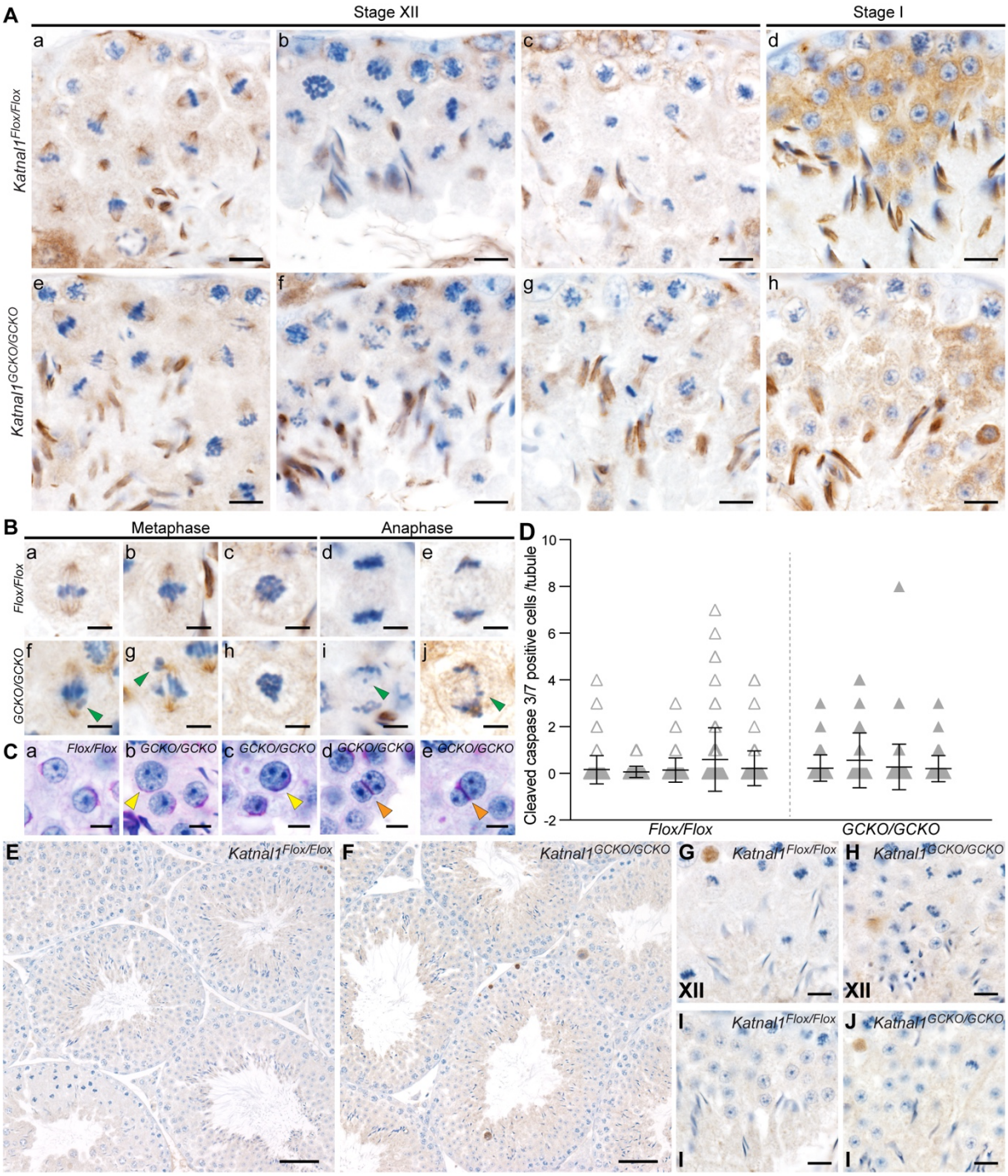

Figure 2: KATNAL1 regulates chromosome alignment, segregation and cytokinesis during male meiosis

(**A-B**) Seminiferous tubule sections immunolabelled for α-tubulin as a component of MTs. Nuclei are counterstained with hematoxylin. Green arrowheads indicate misaligned/lagging chromosomes. (**C**) PAS-stained testis sections showing abnormally large round spermatid nuclei (b,c; yellow arrowhead) and binucleated round spermatids (d-e; orange arrowheads) in

1070 *Katnal1*$^{GCKO/GCKO}$ mice. (**D-J**) Germ cell apoptosis in *Katnal1*$^{GCKO/GCKO}$ mice was assessed by
1071 immunolabelling of seminiferous tubules for cleaved-caspase 3 and 7. The average number of
1072 cleaved-caspase 3 and/or 7 positive germ cells per seminiferous tubule is graphed in **D** and
1073 representative images are shown in **E-G**. In **D** lines represent mean ±SD. A minimum of 80
1074 randomly selected tubules per mouse were counted (n≥3/genotype). Scale bars in **A**-**B**,**G-J** =
1075 10 μm**, C**=5 μm**. E**-**F**= 50 μm.
1076

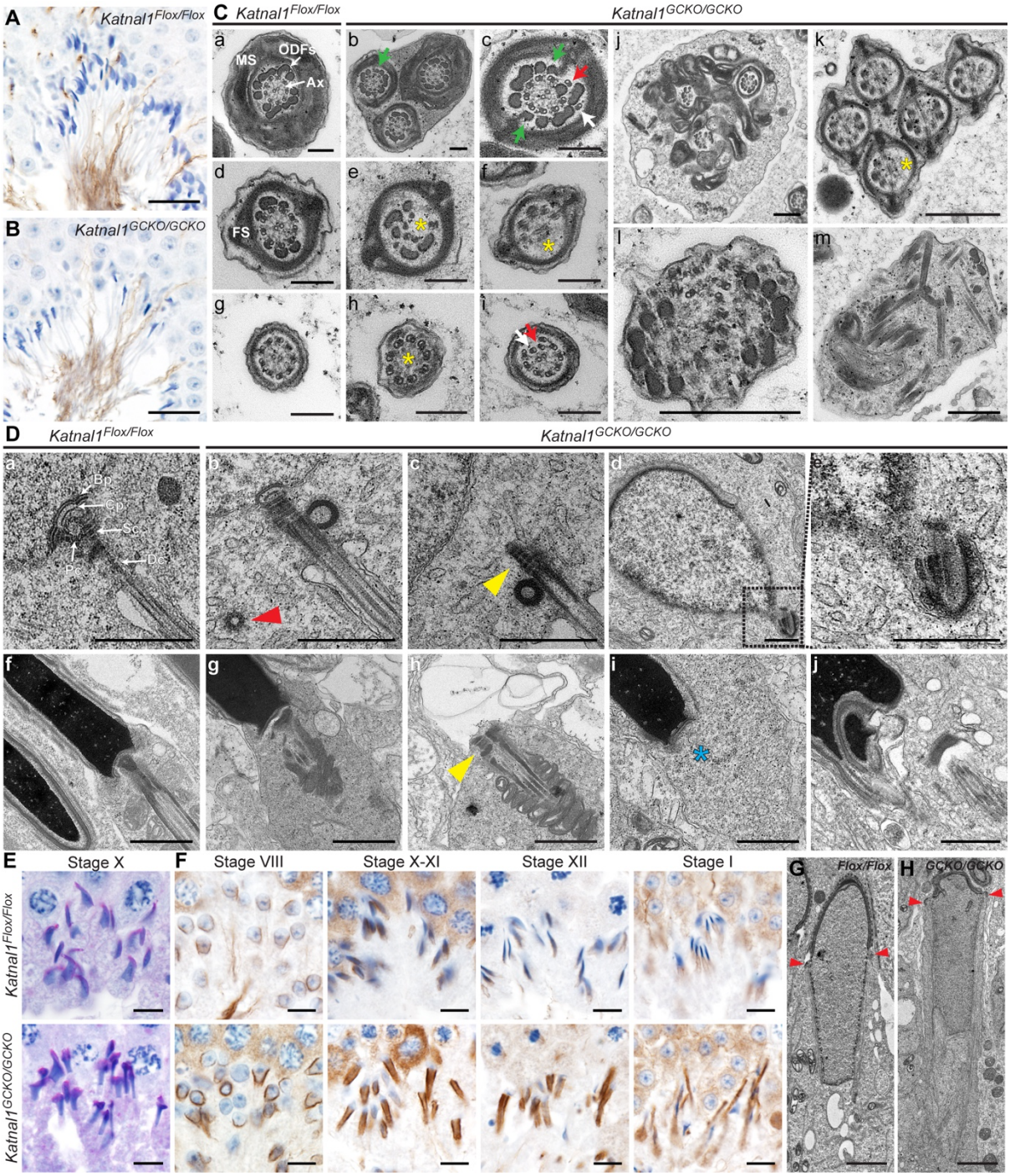

1077

1078 **Figure 3: KATNAL1 is a regulator of flagella formation and the MT manchette in male**

1079 **germ cells**

1080 Testis sections immunolabelled for the axoneme marker acetylated tubulin in *Katnal1*$^{Flox/Flox}$

1081 (**A**) and *Katnal1*$^{GCKO/GCKO}$ (**B**). (**C**) TEM of flagella ultrastructure in cauda epididymal sperm

1082 of *Katnal1*$^{Flox/Flox}$ and *Katnal1*$^{GCKO/GCKO}$ mice. MS= mitochondrial sheath, ODFs = outer dense

1083 fibers, Ax=axoneme FS = fibrous sheath. White arrows indicate supernumerary MT doublets.

1084 Red arrows indicate ectopic MT doublets. Green arrows indicate ectopic ODFs. Yellow
1085 asterisks indicate missing axoneme MT doublets/or central pair. (**D**) TEM of HTCA
1086 ultrastructure in round (**a-e**) and elongated spermatids (**f-j**) in *Katnal1*$^{Flox/Flox}$ and
1087 *Katnal1*$^{GCKO/GCKO}$ mice. Red arrowhead indicated supernumerary centriole. Blue asterisks
1088 indicate absent HTCA. Yellow arrowheads indicate HTCAs are abnormally detached from the
1089 nucleus. (**E**) PAS-stained testis sections showing *Katnal1*$^{Flox/Flox}$ and *Katnal1*$^{GCKO/GCKO}$
1090 elongating spermatids. (**F**) Testis sections immunolabelled for α-tubulin as a maker of the
1091 manchette in *Katnal1*$^{Flox/Flox}$ and *Katnal1*$^{GCKO/GCKO}$ mice. Progressive steps of manchette
1092 formation, migration and dissolution are shown left to right. **(G-H)** TEM showing manchette
1093 structure in *Katnal1*$^{Flox/Flox}$ and *Katnal1*$^{GCKO/GCKO}$ elongating spermatids. Red arrowheads
1094 indicate the perinuclear ring. Scale bars in **A-B** = 20 μm**, Ca-i =** 200 nm, **Cj-m** = 500 nm, **D** =
1095 1 μm, **E-F**=10 μm, **G-H** = 2 μm**.**

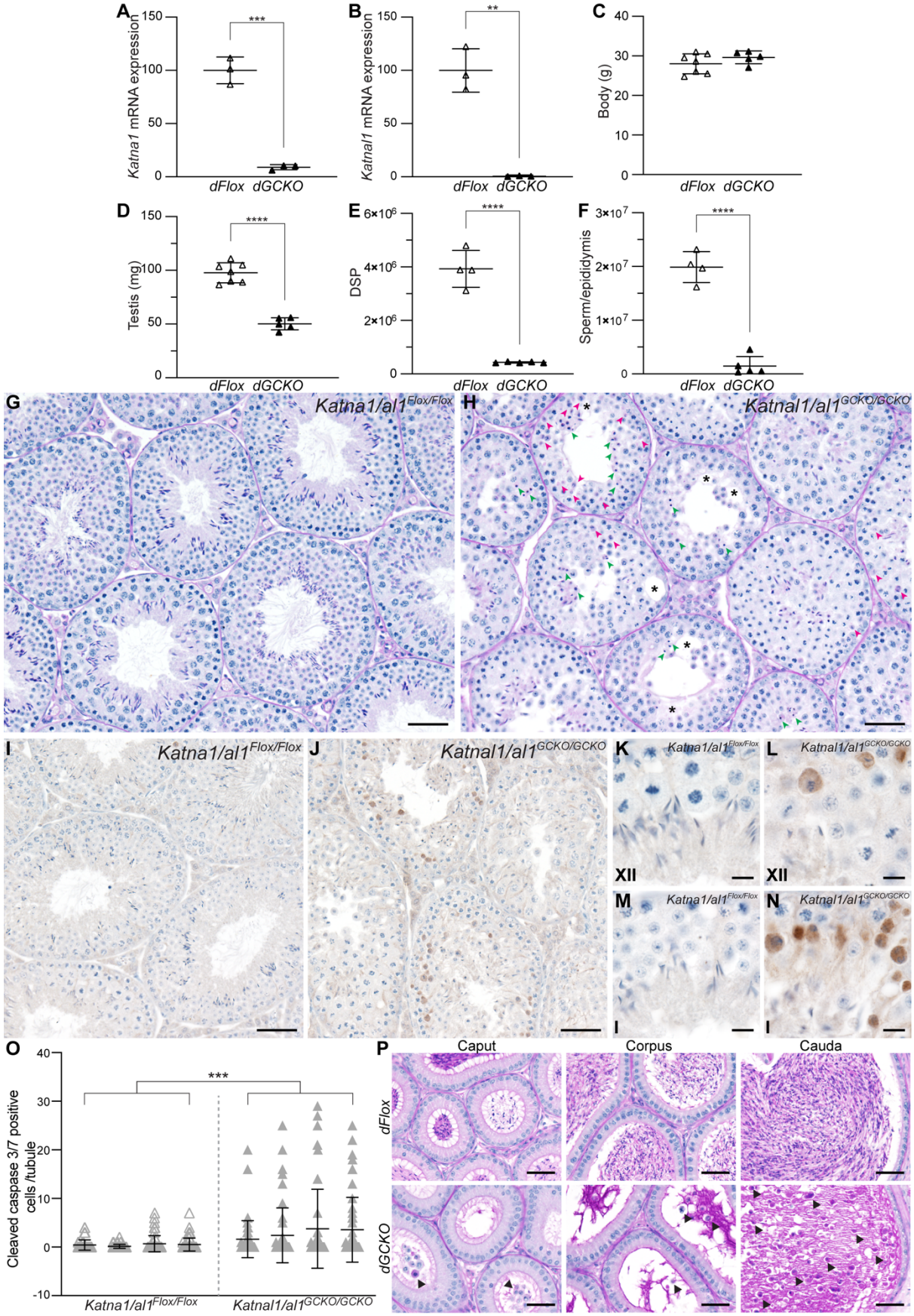
A
Katna1 mRNA expression
150
100
50
0
***
dFlox dGCKO
B
Katnal1 mRNA expression
150
100
50
0
**
dFlox dGCKO
C
Body (g)
40
30
20
10
0
dFlox dGCKO
D
Testis (mg)
150
100
50
0
****
dFlox dGCKO
E
DSP
6×10^6
4×10^6
2×10^6
0
****
dFlox dGCKO
F
Sperm/epididymis
3×10^7
2×10^7
1×10^7
0
****
dFlox dGCKO
G
Katna1/al1^Flox/Flox
H
Katnal1/al1^GCKO/GCKO
I
Katna1/al1^Flox/Flox
J
Katnal1/al1^GCKO/GCKO
K
Katna1/al1^Flox/Flox
XII
L
Katnal1/al1^GCKO/GCKO
XII
M
Katna1/al1^Flox/Flox
I
N
Katnal1/al1^GCKO/GCKO
I
O
Cleaved caspase 3/7 positive cells /tubule
40
30
20
10
0
-10
***
Katna1/al1^Flox/Flox
Katnal1/al1^GCKO/GCKO
P
Caput
Corpus
Cauda
dFlox
dGCKO

1096

1097 **Figure 4: Double germ cell deletion of KATNA1 and KATNAL1 results in a severe**

1098 **oligozoospermia-like phenotype**

1099 qPCR analysis of *Katna1* (**A**) and *Katnal1* (**B**) transcript levels in *Katna1/al1*$^{GCKO/GCKO}$ (black

1100 triangles, *dGCKO*) isolated spermatocytes relative to *Katna1*/*al1*$^{Flox/Flox}$ (white triangles,

1101 *dFlox*) isolated spermatocytes (n≥3/genotype). Body weight (**C**), testis weight (**D**), testis DSP

1102 (**E**), and epididymal sperm content (**F**) in *Katna1/al1*$^{GCKO/GCKO}$ (black triangles) compared to

1103 *Katna1/al1*$^{Flox/Flox}$ controls (white triangles) (n≥3/genotype). Lines represent mean ± SD. PAS-

1104 stained testis (**G-H**) sections from *Katna1/al1*$^{GCKO/GCKO}$ and *Katna1/al1*$^{Flox/Flox}$ mice. Magenta

1105 arrowheads indicate pyknotic spermatocytes and green arrowheads indicate pyknotic

1106 spermatids. Asterisks indicate areas of seminiferous epithelium with vacuoles or devoid of

1107 germ cells. Analysis of germ cell apoptosis in *Katnal1*$^{GCKO/GCKO}$ mice relative to

1108 *Katna1/al1*$^{Flox/Flox}$ mice (**I-O**). Representative images of testis immunolabelling of cleaved-

1109 caspase 3 and 7 are shown in (**I-N**). Roman numerals denote seminiferous tubule stage. The

1110 average number of cleaved-caspase 3 and/or 7 positive germ cells per seminiferous tubule per

1111 mouse is graphed in (**O**). In **O** lines represent mean ±SD. A minimum of 50 randomly selected

1112 tubules per mouse were counted (n≥3/genotype). PAS-stained epididymis sections (**P**) from

1113 *Katna1/al1*$^{GCKO/GCKO}$ and *Katna1/al1*$^{Flox/Flox}$ mice. Scale bars in **G-J** = 50 µm, in **K-N** = 10 µm,

1114 **P** = 40 µm. **P*<0.05 , ***P*<0.01, ****P*<0.01, *****P*<0.001.

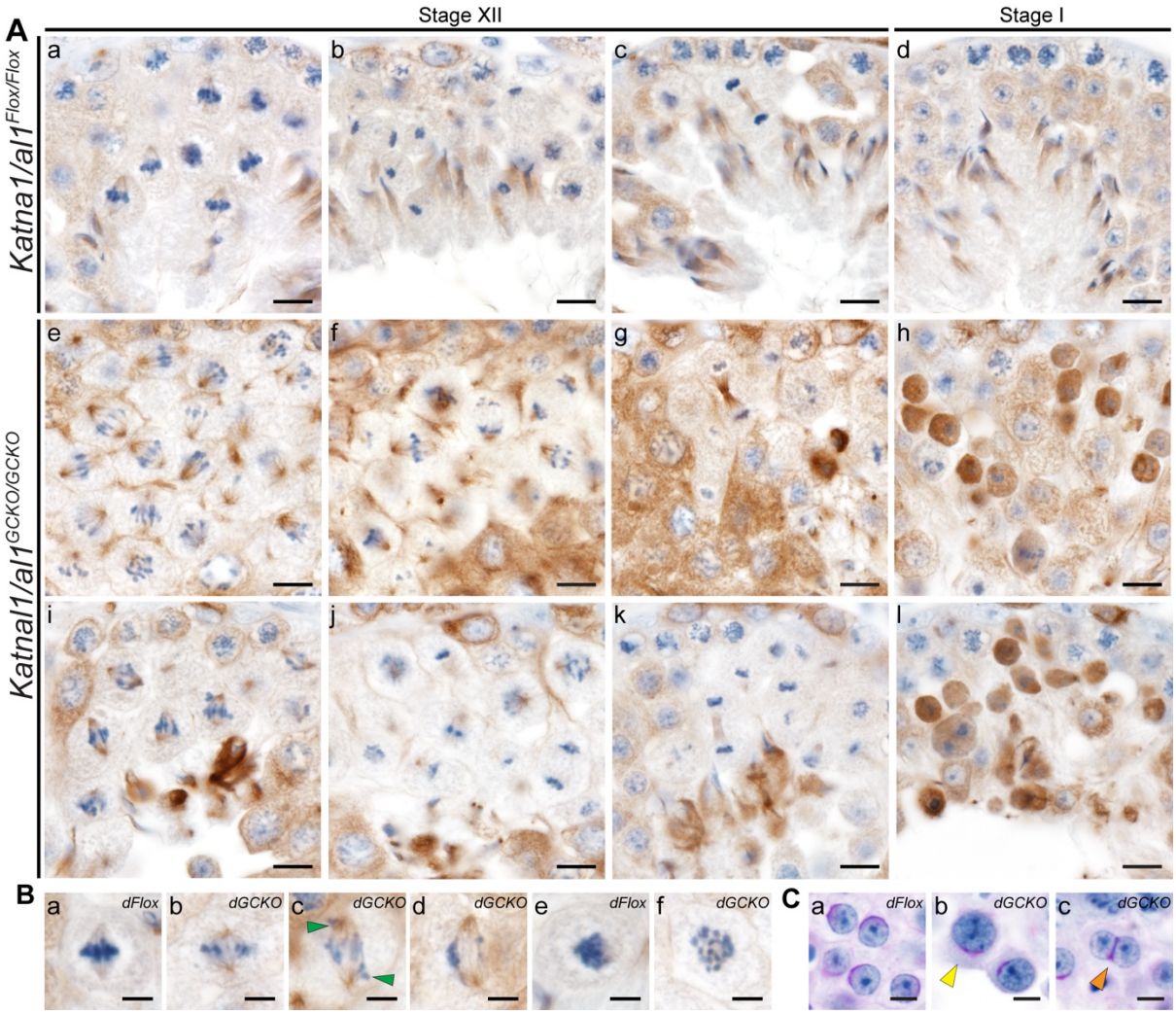

1115

1116 **Figure 5: KATNA1 and KATNAL1 compensate for each other in male meiosis**

1117 (**A-B**) *Katnal1/al1*$^{Flox/Flox}$ (*dFlox*) and *Katna1/al1*$^{GCKO/GCKO}$ (*dGCKO*) seminiferous tubule

1118 sections immunolabelled for MTs (α-tubulin). Nuclei are counterstained with hematoxylin.

1119 Green arrowheads indicate misaligned/lagging chromosomes. (**C**) PAS-stained

1120 *Katnal1/al1*$^{Flox/Flox}$ (*dFlox*) and *Katna1/al1*$^{GCKO/GCKO}$ (*dGCKO*) testis sections showing

1121 abnormally large round spermatid nuclei (b; yellow arrowhead) and binucleated round

1122 spermatids (c; orange arrowheads) in *Katna1/al1*$^{GCKO/GCKO}$ mice. Scale bars in **A**= 10 µm, in

1123 **B-C**= 5 µm.

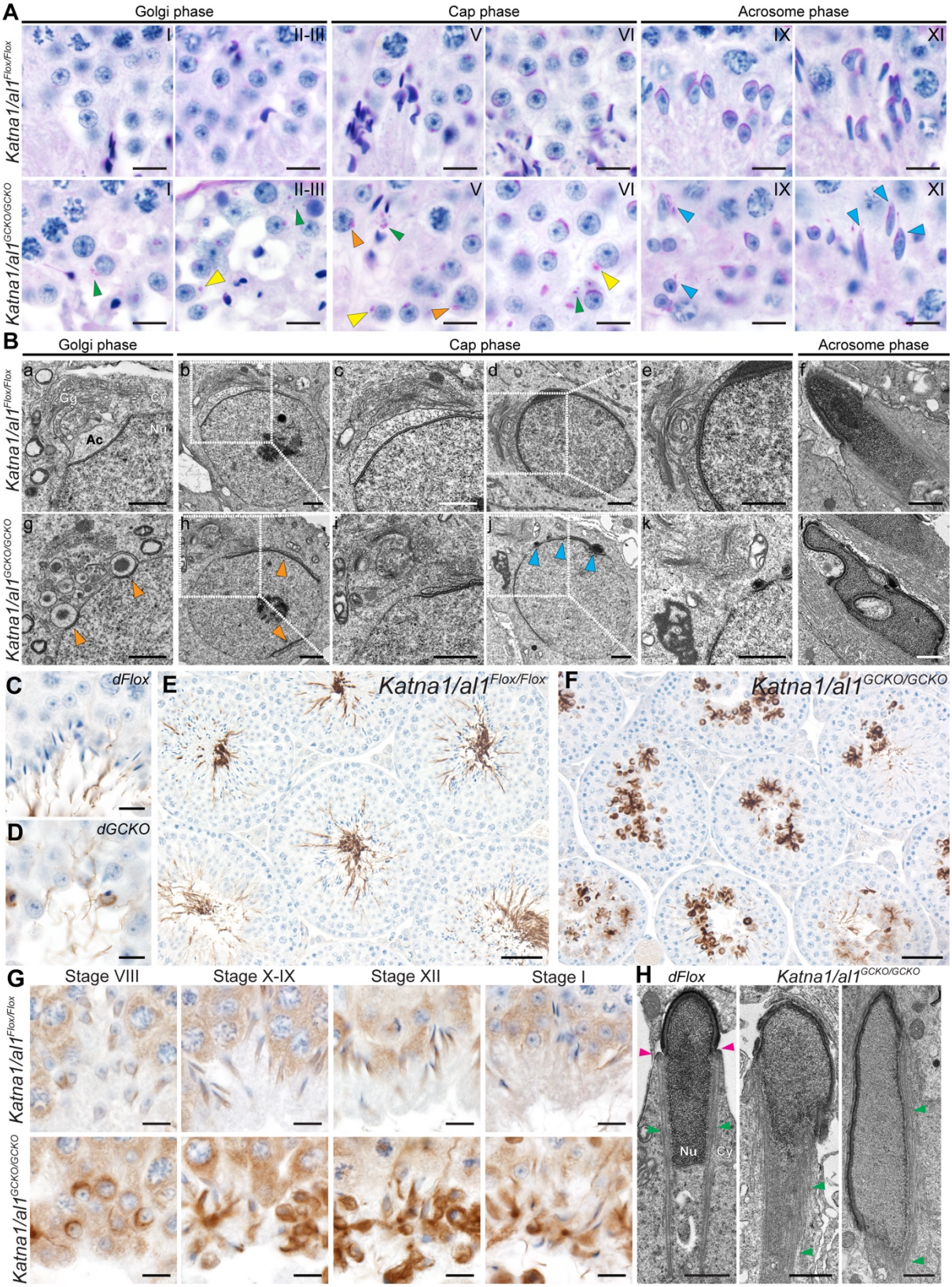

Figure 6: **KATNA1 and KATNAL1 compensation in spermatid acrosome formation and MT regulation**

1127 (**A**) PAS-stained testis sections showing acrosome formation in *Katna1/al1*$^{Flox/Flox}$ and
1128 *Katna1/al1*$^{GCKO/GCKO}$ mice. Progressive steps of acrosome formation are shown left to right.
1129 Roman numerals denote seminiferous tubule stage. Orange arrowheads indicate nuclei with
1130 more than one proacrosomal vesicle attached. Yellow arrowheads indicate acrosomal vesicles
1131 not attached to the nucleus. Green arrowheads indicate ectopic PAS positive vesicles
1132 abnormally dispersed in round spermatid cytoplasm. Blue arrowheads indicate elongating
1133 spermatids with abnormal gaps/fragmentation of the acrosomes. (**B**) Electron micrographs
1134 showing acrosome and Golgi apparatus ultrastructure in *Katna1/al1*$^{Flox/Flox}$ and
1135 *Katna1/al1*$^{GCKO/GCKO}$ mice. Orange arrowheads indicate supernumerary site of acrosome
1136 formation. Blue arrowheads indicate numerous small unfused acrosomal vesicles docked at the
1137 nuclear membrane/fragmentation of the acrosome. (**C-F**) *Katna1/al1*$^{Flox/Flox}$ (*dFlox*) and
1138 *Katna1/al1*$^{GCKO/GCKO}$ (*dGCKO*) mouse testis sections immunolabelled for the sperm tails
1139 marker acetylated tubulin. (**G**) *Katna1/al1*$^{Flox/Flox}$ and *Katna1/al1*$^{GCKO/GCKO}$ testis sections
1140 immunolabelled for α-tubulin as a maker of the manchette. Progressive steps of manchette
1141 formation, migration and dissolution are shown left to right. TEM showing nuclear and
1142 manchette morphology in *Katna1/al1*$^{Flox/Flox}$ (*dFlox*) and *Katnal1*$^{GCKO/GCKO}$ mouse elongating
1143 spermatids. Red arrowheads indicate the perinuclear ring. Blue arrowheads indicate MTs. Scale
1144 bars in **A, C-D** = 10 µm, **B,H** = 1 µm, **E-F** = 50 µm, **G**=10 µm. Nu = Nucleus, Cy =cytoplasm
1145 Gg=Golgi apparatus, Ac=acrosome.

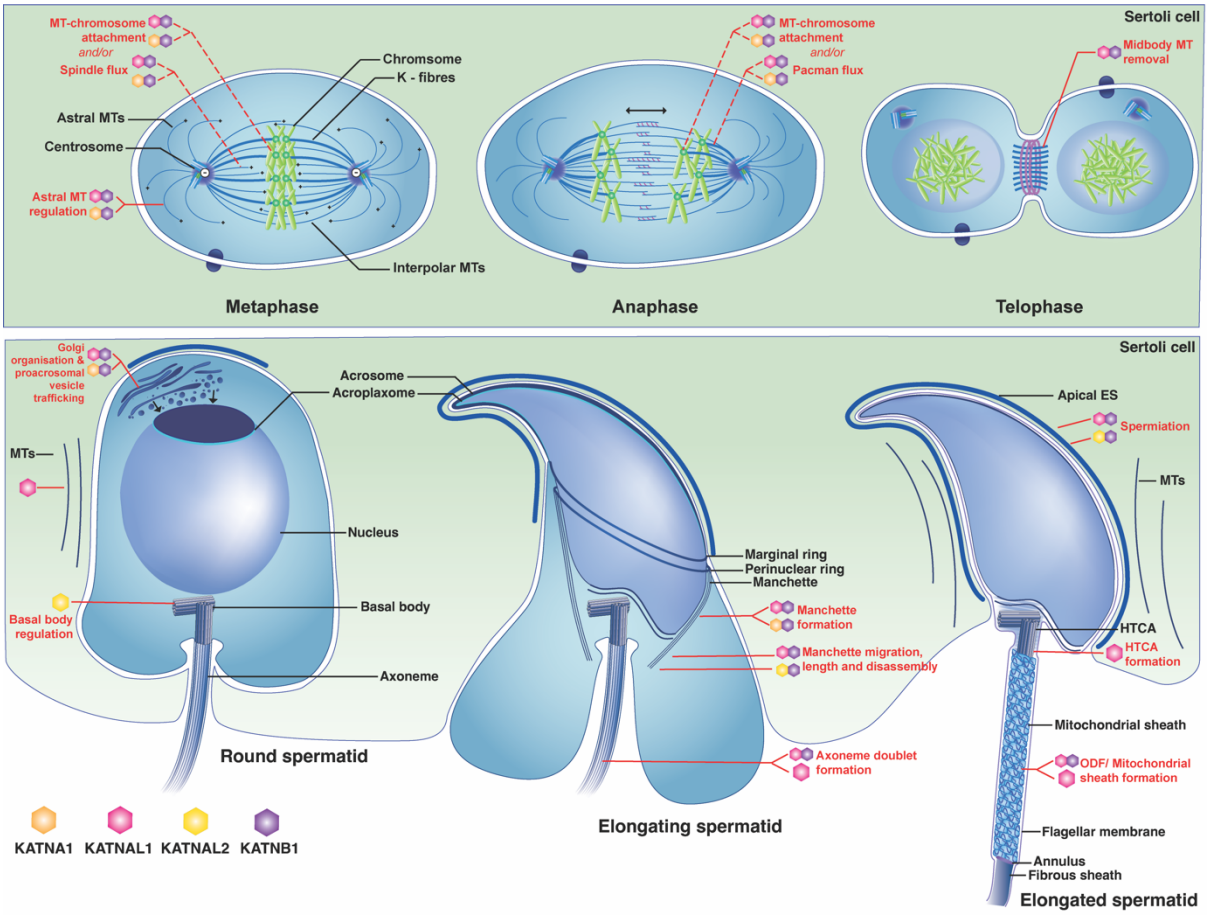

1146

1147 **Figure 7: Proposed model of katanin regulation of spermatogenesis**

1148 KATNB1-independent and -dependent functions of each katanin A-subunit during male germ
1149 cell development are depicted based on the data defined herein and defined for KATNAL1
1150 Sertoli cell function in [13], for KATNAL2 in [5] and KATNB1 defined in [11,12]. A shared line
1151 indicates two complexes have redundant/compensatory function in the process indicated.
1152 HTCA = head to tail coupling apparatus, MTs = microtubule, ODF = outer dense fibers.

1153